Journal of Dynamics, Monitoring and Diagnostics, 2024, 3, 112-142
https://doi.org/10.37965/jdmd.2024.517

ISTP
RESEARCH ARTICLE

Identification of the Asymmetric Transmission Error and Gear Mesh Dynamic Parameters using Full-Spectrum Responses in a Geared-Rotor System

Bhyri Rajeswara Rao and Rajiv Tiwari
Indian Institute of Technology Guwahati, Guwahati, Assam, India

(Received 15 February 2024; Revised 17 May 2024; Accepted 28 May 2024; Published online 29 May 2024)

Abstract: A dominant source of vibration in geared-rotor systems is the gear mesh fault parameters. They include the asymmetric transmission error (TE), phases of TE, the gear mesh stiffness, the gear mesh damping, and the gear runouts. The present work deals with the experimental identification of the aforementioned parameters. A mathematical model of a geared-rotor system has been developed using Lagrangian dynamics. Equations of motion are transformed into the frequency domain using the full-spectrum response analysis. These transformed equations are used to develop an identification algorithm (IA) based on least-squares fit to estimate the TE and gear mesh dynamic parameters. The system IA is initially verified using numerical simulations. The robustness of the algorithm is checked by introducing white Gaussian noise in the simulated responses. A geared-rotor experimental rig was developed and used to measure responses at gear locations in two orthogonal directions. Measured responses are transformed in the frequency domain using the full-spectrum analysis and used in the present novel IA to identify the gear parameters. The identified parameters are validated by comparing the numerically generated full-spectrum response using experimentally estimated parameters and that from the experimental rig.

Keywords: Full-spectrum; Geared-rotor system; Identification; Multiple faults; Runouts; Transmission error

Nomenclature

Symbol	Description
C_1	Center of rotation of pinion
C_2	Center of rotation of gear
c_m	Gear mesh damping along the line of action (LOA)
c_{s1}	Damping of input rotor
c_{s2}	Damping ratio of output rotor
e_f	Variable transmission error (TE)
$e_{f_{xi}}(t)$	Harmonics of variable TE in x-direction
$e_{f_{yi}}(t)$	Harmonics of variable TE in y-direction
e_g	Gear runout
e_{lg}	Gear runout along the LOA
e_{lp}	Pinion runout along the LOA
e_m	Mean TE
e_p	Pinion runout
$e_x(t)$	Dynamic TE in x-direction
$e_y(t)$	Dynamic TE in y directions
G_1	Center of gravity of pinion
G_2	Center of gravity of gear
$\boldsymbol{i}$	Number of harmonics of TE
k_m	Gear mesh stiffness along the LOA
k_{s1}	Stiffness of the input shaft
k_{s2}	Stiffness of the output shaft
m_1	Mass of the pinion
m_2	Mass of the gear
m_{avg}	Average mass of gear mesh
N_1	Rotational speed of the input shaft
N_2	Rotational speed of the output shaft
O_1	Ideal center of the pinion
O_2	Ideal center of the gear
r_{b1}	Base radius of the pinion
r_{b2}	Base radius of the gear
r_{l1}	Deflection of input shaft along the LOA
r_{l2}	Deflection of output shaft along the LOA
Z_p	Number of teeth on the pinon
Z_g	Number of teeth on the gear
$U_g = m_2 e_g$	Mass unbalance at the gear
$U_p = m_1 e_p$	Mass unbalance at the pinion
α	Angle of LOA orientation with y-axis
δ	Deformation of the meshing teeth along the LOA
δ_x	The component of δ in x-direction
δ_y	The component of δ in y-direction
ϕ_d	Initial phase of the drive
ϕ_g	Initial phase of the gear
ϕ_l	Initial phase of the load
ϕ_p	Initial phase of the pinion
φ_{z1}	The angular displacement of the gear
φ_{z2}	The angular displacement of the pinion
φ_{zd}	The angular displacement of drive
φ_{zl}	The angular displacement of load
ω_e	Frequency of gear mesh
$\omega_e = Z_p\omega_p = Z_g\omega_g;$	
$\omega_e = 2\pi N_p Z_p/60 = 2\pi N_g Z_g/60$	
ω_g	Angular speed of the gear
ω_p	Angular speed of the pinion
ζ_m	Gear mesh damping ratio

I. INTRODUCTION AND LITERATURE REVIEW

The complex nature of rotating machinery fascinated a lot of researchers to study their dynamic behavior. These studies resulted in the design of lighter, high-speed and exceptionally reliable automotive, aerospace and other

Corresponding author: Rajiv Tiwari (e-mail: rtiwari@iitg.ernet.in).

industrial machinery. Geared-rotor systems are the most commonly used torque-carrying members in most of the mechanical and electrical equipment. Gears are considered as dominant source of vibration due to their deviations from perfect conjugate profile and the dynamic nature of gear contact between flanks of mating gears. The parameters that cause this profile deviation are considered as the transmission error (TE), gear mesh stiffness and gear runout errors, individually or in combination. These dynamic effects may sometimes cause catastrophic failure of mechanical systems and subassemblies attached to the supporting structure. Estimation of these gear parameters is having paramount importance [1].

Several researchers studied the identification of rotating machinery faults, such as gear faults, misalignments, residual unbalances, shaft bow, shaft cracks, motor faults, and bearing faults using system mathematical models [2–4]. In these attempts, authors used the analytical, transfer matrix and finite element (FE) methods. Wherein, the fault models with unknown parameters are considered. Through least-squares or other fitting techniques, the unknown fault parameters are estimated with the help of system responses. Some researchers used feature extraction techniques, conventional neural networks, discrete wavelet transform, and thermal images [5–9].

Plenty of researchers studied geared-rotor vibration through numerous mathematical models. Most of the researchers considered TE as an excitation source for the gear vibration problem. TE is specified at the pitch point of the gear mesh, and it is mathematically expressed as a change in driven gear position with respect to the position of a perfect gear drive. The perfect gear drive is free from any geometrical deviations from its conjugate profile. Several researchers presented fundamental concepts of TE and its measurement techniques [10–12]. Özgüven and Houser [13] reviewed works on mathematical models used in gear dynamics. They gave insights into the sources of the mesh excitation and its contribution to the system excitation, pertaining to the gear noise. Houser [14] published the state of the art by summarizing research works on the contribution of various sources of gear mesh excitations to gear noise. Kahraman *et al.* [15] presented FE modeling of geared-rotor mounted on flexible bearings with a combination of TE excitation and constant gear mesh stiffness.

Wadkar and Kajale [16] studied geared-rotor natural frequencies and modes shapes. Also, the reliability of geared-rotor system using the time-varying mesh stiffness was investigated. Mohammed *et al.* [17] proposed an improved mesh stiffness calculation for the purpose of fault detection in geared rotors using vibration signals. Li *et al.* [18] studied coupled lateral–torsional–axial vibration problem of helical gears mounted on flexible bearings using a system model approach. Zhou *et al.* [19] analyzed a coupled vibration of a spur gear pair considering the TE and presented vibration response using a three-dimensional frequency spectrum. They studied the influence of eccentricity, speed, and bearing clearance on the nonlinear response. Temis *et al.* [20] studied gear vibration problem with proportional viscous damping by considering the time-varying mesh stiffness and the tooth separation. Mohamed *et al.* [21] presented the dynamic behavior of geared systems with multiple cracks using a model-based approach. Rao and Ganti [22] presented a case study to mitigate gear whine in 6-speed automotive transmission using three-dimensional multi-body dynamics simulation by exciting the loaded gear pair with TE. They also suggested procedures for mitigation of the gear whine.

To analyze the geared-rotor response in the frequency domain, the signal processing techniques are very important. It separates response due to different fault frequencies and helps in the identification of TE and other gear mesh faults. Traditional fast Fourier transform (FFT) fails to provide the direction of the precession of the pinon and gear harmonics with respect to the direction of the drive shaft. Southwick [23] presented the full-spectrum analysis, which unwraps the traditional FFT spectrum into the forward and backward whirl frequencies. Full-spectrum response is suitable for analyzing the response of the geared-rotor system as it is an augmented version of the Campbell diagram. Qu *et al.* [24] studied vibration measurement of large machinery by short-period Fourier transform and Wigner distribution to nullify the shortfalls in conventional FFT methods. Southwick [25] studied the response of a rotor using full-spectrum response for obtaining the asynchronous and synchronous vibrations. He investigated the ellipticity of whirling orbits under various conditions that paved the motivation for the progress to full-spectrum analysis. Goldman and Muszynska [26] presented a method for the detection of various rotating machinery faults with full-spectrum response. They also presented the phase correlation of rotor orbits in the horizontal and vertical spectrum components. Bachschmid *et al.* [27] analyzed rotating machinery vibrations using full-spectrum response with shape and directivity index method for analyzing the ellipticity of filtered orbit. Tuma and Bilos [28] studied a rotor mounted on a fluid film bearing to identify fluid-induced instability and whirl frequency components with full-spectrum response plots. Patel and Darpe [29] investigated cracked rotors using full-spectrum response for the identification of the crack rub with the directional nature of higher harmonics. Shravankumar and Tiwari [30] studied the model-based crack identification in cracked rotors with full-spectrum response plots.

Hong and Dhupia [31] demonstrated a time domain approach to identify the gearbox faults using measured response from an experimental rig. Sawalhi and Randall [32] presented a method for the identification of teeth count of two parallel stages of gears without speed reference signal under variable speed conditions. Feng *et al.* [33] proposed an order spectrum analysis method based on the iterative generalized demodulation for the characteristic frequency identification in a faulty planetary gearbox. Dogan and Karpat [34] presented a dynamic transmission error (DTE)-based numerical fault detection model using FE analysis for crack detection in spur gears with asymmetric teeth. Benatar *et al.* [35] presented a set of motion TE data for a family of helical gears having different profile and lead modifications operated under both low-speed (quasi-static) and dynamic conditions. Celikay [36] studied a subharmonic resonance observed in spur gear pairs as a parametrically excited system. The stiffness at the gear contact interface that couples the gear bodies is periodically time-varying due to the fluctuation of number of tooth pairs in contact. Flek *et al.* [37] presented the time-varying stiffness of spur gears in the dynamic model of transmission systems as an internal excitation of the dynamic system.

Chin *et al.* [38] proposed a TE-based method for the estimation of gear root crack depth as an indicator of severity. Xue *et al.* [39] presented a gear system dynamic model for the nonstationary operating condition using the

iterative convergence of the tooth mesh stiffness and demonstrated the effect of gear tooth crack on the resultant dynamic response for the nonstationary condition. Poletto *et al.* [40] presented the identification of gear wear damage using topography analysis. Dai *et al.* [41] developed a simulation model to investigate the impact of defective bearings on the mesh characteristics of gear pairs. Talakesh *et al.* [42] presented experimental and analytical methods to calculate the time-varying mesh stiffness for healthy and cracked straight bevel gear systems. Dong *et al.* [43] presented a mediator algorithm between simulation and experiment to identify the error excitation in gear systems. The authors also proposed a signal processing procedure to eliminate the phase difference and improve the signal-to-noise ratio. Koutsoupakis [44] presented a damage identification and condition monitoring (CM) method based on CNNs and validated on an experimental two-stage gearbox. The CM-CNN was trained on numerical data (PSDs) generated by repetitive simulations of an optimized MBD model of the actual structure with randomly sampled parameters.

From the literature survey, very limited literature is found on the identification of the TE of a gear mesh using vibration signal. This research work focused on a novel model-based approach for the quantitative identification of the TE along with other gear dynamic parameters. In this direction, the authors recently presented their work [45], where the response of geared-rotor system is analyzed using the full-spectrum response to detect qualitatively the novel asymmetric TE of variable components of TE. However, the authors have not attempted to have quantitative estimates of the TE. In this work, the authors have developed an identification procedure based on geared-rotor model of [45] to estimate the novel asymmetric TE along with the mean TE, phases of variable TE, gear mesh stiffness, gear mesh damping, and gear runouts using the full-spectrum response.

The content provided in the following sections is as follows. Section II gives a brief on the modeling of geared-rotor system, gear mesh fault parameters, and the derived equations of motion using the Lagrangian dynamics. Section III depicts the formulation to transform equations of motion from time domain to frequency domain. Section IV details the development of an identification algorithm (IA) for quantitative identification of gear mesh parameters. Section V presents the numerically simulated full-spectrum responses of geared-rotor system. Section VI describes the numerical testing of IA. Section VII has information about the experimental rig. Section VIII describes full-spectrum response analyses from the experimental rig response measurements. Section IX describes the identification of gear mesh DTE parameters using experimental rig full-spectrum responses. Section X presents the validation of geared-rotor system model and the IA. Section XI summarizes the conclusions of the present work. Appendices A and B give frequency domain formulation transformation of equations of motion

II. GEARED-ROTOR SYSTEM MODEL AND GEAR MESH FAULT PARAMETERS

In this section, descriptions are presented related to the formulation of equations of motion [45], which are used for the development of the identification of TE and other uncertain system fault parameters. The shaft supports are assumed to be rigid in transverse directions, and shafts and gears are also considered to be rigid in the torsion mode of vibration that gives the scope of ignoring the torsional vibration of the geared system. This assumption also eliminated the nonlinearities associated with resulting geared-rotor equations of motion. This approach provides the opportunity to study more about gear transmission dynamics problem with matured linear mathematical techniques of transverse vibration. A four-DOF system model is developed for modeling gear transverse vibration problem with the TE as shown in Fig. 1(a) and 1(b). The system model has two shafts of lengths l_1 and l_2 and a motor drive connecting to the input shaft with a rigid coupling. The input shaft carries a pinion, and the output shaft carries a gear. Both the pinion and the gear are mounted at the mid-span of the uniform flexible shafts to have a gear mesh. The output shaft is loaded with the required torque to load the gear pair so that they remain in contact during operation without separation.

To consider the fluctuation in gear mesh stiffness due to deviation from the conjugate gear profile, the static

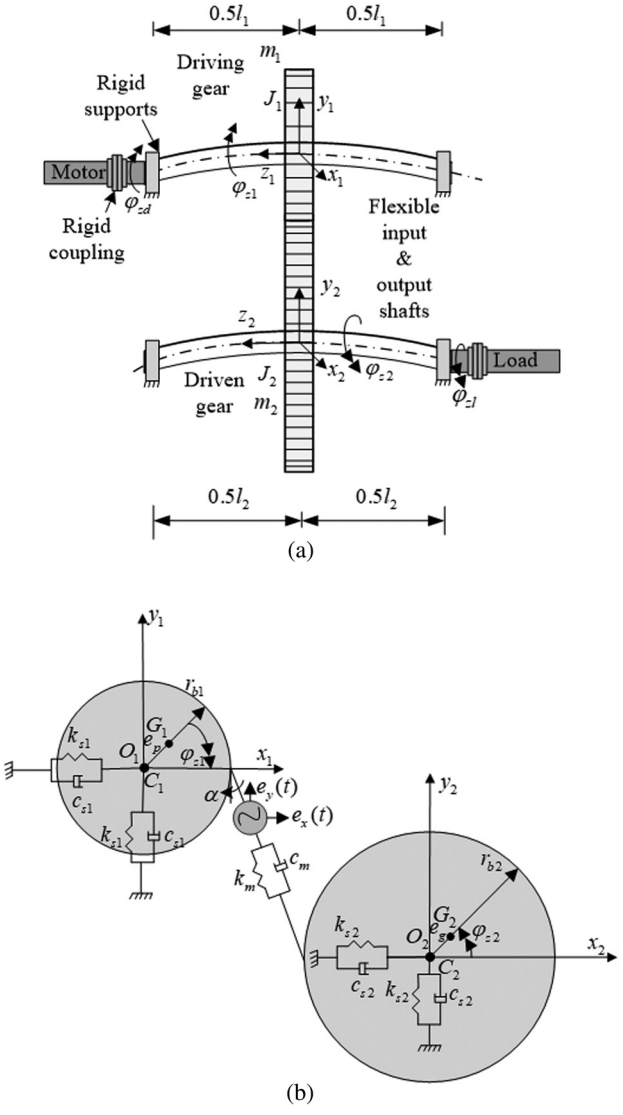

Fig. 1. (a) Overall geared-rotor system; (b) The geared-rotor system model.

transmission error (STE) is incorporated. This paper uses the orientation of the line of action (LOA) at an angle α with y-axis [45], as shown in Fig. 1(b), to model the meshing of gears between two parallel shafts in a realistic power transmission. This work also assumes two different TEs in two lateral orthogonal directions to consider the different excitations in two orthogonal directions ($e_x(t)$ and $e_y(t)$). It helps in studying the forward and backward whirl features of gear mesh when it is loaded. The angular displacements of the drive, pinion, gear, pinion, and load are given, respectively, as:

$$\varphi_{zd}(t) = \omega_p t + \phi_d; \qquad \varphi_{z1}(t) = \omega_p t + \phi_p;$$
$$\varphi_{z2}(t) = \omega_g t + \phi_g; \qquad \varphi_{zl}(t) = \omega_g t + \phi_l \tag{1}$$

Herein, ω_p and ω_g are the spin speed of the pinion and the gear, respectively, ϕ is the initial phase, and subscripts d denotes the drive, p denotes the pinion, g denotes the gear, and l denotes the load. Also, the gyroscopic effect is not significant in this formulation as the pinion and the gear are fixed at the mid-span of the shafts. Geometric relations are given as:

$$x_p = x_1 + e_p\cos(-\varphi_{z1}); \quad y_p = y_1 + e_p\sin(-\varphi_{z1});$$
$$x_g = x_2 + e_g\cos\varphi_{z2}; \quad y_g = y_2 + e_g\cos\varphi_{z2} \tag{2}$$

where (x_1, y_1) are the displacements of the center of pinion, (x_2, y_2) are the displacements of the center of gear, (x_p, y_p) are the positions of the center of gravity of the pinion, (x_g, y_g) are the positions of the center of gravity of the gear, and e_p and e_g are runouts of the pinion and the gear, respectively. On substituting equation (1) into equation (2), we get

$$\begin{aligned} x_p &= x_1 + e_p\cos(-\omega_p t - \phi_p);\\ y_p &= y_1 + e_p\sin(-\omega_p t - \phi_p);\\ x_g &= x_2 + e_g\cos(\omega_g t + \phi_g);\\ y_g &= y_2 + e_g\sin(\omega_g t + \phi_g) \end{aligned} \tag{3}$$

The gear runouts generate unbalanced force in the pinion and the gear; in addition, they give rise to relative deformation of shafts during the torque transfer. The STE along with the runout errors that contribute to no-load transmission error (NLTE) constitute the DTE. The DTE excites the gear drive at the pitch point, which is assumed as the sum of mean and variable components with their initial phases. The difference of STE from tooth-to-tooth is not considered in this model to avoid complex equations for derivation. As the LOA is slanted by an angle α with y-direction, the DTE is modeled to excite the gear mesh in x and y directions on the exterior of the contact region created at the pitch point due to gear mesh profile deviation in the complete mesh cycle (start of engagement of teeth in a gear mesh to end of engagement of teeth).

It is found in the literature [15] that while modeling DTE, sinusoidal excitation along the pressure line is given at the gear mesh frequency by neglecting the initial phase. In this work, similar to the work of the authors [45], the initial phase is included in the excitation. Apart from a constant term, the sine and cosine variations with an initial phase and higher harmonics of the gear mesh frequency are also included. As proposed by the authors in their work [45] and supported by the literature [15], in the present work, the variable gear mesh stiffness force has been modeled with a constant mesh stiffness multiplied by displacement in the form of loaded STE, which gives external forcing as in Kahraman *et al.* [15]. Also, it is assumed that the relative deformation of gears is completely transformed into elastic deformation on the surface of teeth. The dynamics of a pair of gears are mathematically modeled as disks. These disks at their pitch circle radius joined using spring and damper having gear mesh stiffness (k_m) and gear mesh damping (c_m), respectively, along the LOA. The LOA is tangent to the base circle of gears to ensure the contact of the teeth surface during power transmission. So, the displacement (δ) between the pinion and gear along the LOA is given as:

$$\delta = r_{l1} - r_{l2} + e_{lp} - e_{lg} + r_{bp}\varphi_{zp} - r_{bg}\varphi_{zg} - e(t) \tag{4}$$

where r_{l1} and r_{l2} are elastic deformations of the input and output shafts; e_{lp} and e_{lg} are gear runouts of pinion and gear along LOA. For a constant gear ratio, the fifth and sixth terms of above equation remain same and together they become zero. Along the LOA, the dynamic gear mesh force is given in equation (5) as:

$$F_m = c_m\dot{\delta} + k_m\delta \tag{5}$$

where k_m and c_m denote the average mesh stiffness and damping along the LOA, respectively. The DTE modeled in the x and y directions depict a practical state of power transmission as shown in Fig. 1(b). The components of δ in the x and y directions, from equations (3) and (4), are given as:

$$\begin{aligned} \delta_x = x_1 - x_2 &+ e_p\cos(\omega_p t + \phi_p)\\ &- e_g\cos(\omega_g t + \phi_g) - e_x(t) \end{aligned} \tag{6}$$

$$\begin{aligned} \delta_y = y_1 - y_2 &- e_p\sin(\omega_p t + \phi_p)\\ &- e_g\sin(\omega_g t + \phi_g) - e_y(t) \end{aligned} \tag{7}$$

The dynamic gear mesh force given in equation (5) is resolved in the x and y components. The elastic deformation in the contact region at the pitch point is given by equations (6) and (7). The components of DTE $e_x(t)$ and $e_y(t)$ in the x and y directions are modeled as a mean value and a fluctuating part [45] and can be given as:

$$e_x(t) = e_m + e_{f_x}(t); \qquad e_y(t) = e_m + e_{f_y}(t) \tag{8}$$

with

$$e_{f_x}(t) = \sum_{i=1}^{n} e_{f_{xi}}\sin(i\omega_e t + \phi_{e_{xi}});$$
$$e_{f_y}(t) = \sum_{i=1}^{n} e_{f_{yi}}\sin(i\omega_e t + \phi_{e_{yi}}) \tag{9}$$

The displacement vector of the centers of shafts in geared rotors is given as:

$$q_i = \begin{bmatrix} x_1 & y_1 & x_2 & y_2 \end{bmatrix}^T \tag{10}$$

where subscripts 1 and 2 refer to the pinion and gear shafts, respectively. Using the Lagrangian dynamics, the equations of motion are derived and presented in the matrix form [45], which contain forces from the TE, and the unbalances and runouts are given as:

$$\mathbf{M}\ddot{\boldsymbol{\eta}}(t) + \mathbf{C}\dot{\boldsymbol{\eta}}(t) + \mathbf{K}\boldsymbol{\eta}(t) = \mathbf{f}(t) \tag{11}$$

with

$$\mathbf{M}=\begin{bmatrix} m_1 & 0 & 0 & 0 \\ 0 & m_1 & 0 & 0 \\ 0 & 0 & m_2 & 0 \\ 0 & 0 & 0 & m_2 \end{bmatrix}; \qquad \mathbf{C}=\begin{bmatrix} c_{s1}+c_m & 0 & -c_m & 0 \\ 0 & c_{s1}+c_m & 0 & -c_m \\ -c_m & 0 & c_{s2}+c_m & 0 \\ 0 & -c_m & 0 & c_{s2}+c_m \end{bmatrix}; \tag{12}$$

$$\mathbf{K}=\begin{bmatrix} k_{s1}+k_m & 0 & -k_m & 0 \\ 0 & k_{s1}+k_m & 0 & -k_m \\ -k_m & 0 & k_{s2}+k_m & 0 \\ 0 & -k_m & 0 & k_{s2}+k_m \end{bmatrix}; \qquad \boldsymbol{\eta}=\begin{Bmatrix} x_1 \\ y_1 \\ x_2 \\ y_2 \end{Bmatrix}; \tag{13}$$

$$\mathbf{f}(t)=\begin{Bmatrix} f_{x1}(t) \\ f_{y1}(t) \\ f_{x2}(t) \\ f_{y2}(t) \end{Bmatrix}=\begin{Bmatrix} m_1 e_p \omega_p^2 \cos(\omega_p t+\phi_p)+c_m\left\{e_p\omega_p \sin(\omega_p t+\phi_p)-e_g\omega_g \sin(\omega_g t+\phi_g)+\dot{e}_x(t)\right\} \\ +k_m\left\{-e_p\cos(\omega_p t+\phi_p)+e_g\cos(\omega_g t+\phi_g)+e_x(t)\right\}+c_{s1}e_p\omega_p\sin(\omega_p t+\phi_p)-k_{s1}e_p\cos(\omega_p t+\phi_p) \\ -m_1 e_p \omega_p^2 \sin(\omega_p t+\phi_p)+c_m\left\{e_p\omega_p \cos(\omega_p t+\phi_p)+e_g\omega_g \cos(\omega_g t+\phi_g)+\dot{e}_x(t)\right\} \\ +k_m\left\{e_p\sin(\omega_p t+\phi_p)+e_g\sin(\omega_g t+\phi_g)+e_y(t)\right\}+c_{s1}e_p\omega_p\cos(\omega_p t+\phi_p)+k_{s1}e_p\sin(\omega_p t+\phi_p)-m_1 g \\ m_2 e_g \omega_g^2 \cos(\omega_g t+\phi_g)-c_m\left\{e_p\omega_p \sin(\omega_p t+\phi_p)-e_g\omega_g \sin(\omega_g t+\phi_g)+\dot{e}_x(t)\right\} \\ -k_m\left\{-e_p\cos(\omega_p t+\phi_p)+e_g\cos(\omega_g t+\phi_g)+e_x(t)\right\}+c_{s1}e_p\omega_p\cos(\omega_p t+\phi_p)+k_{s1}e_p\sin(\omega_p t+\phi_p) \\ m_2 e_g \omega_g^2 \sin(\omega_g t+\phi_g)-c_m\left\{e_p\omega_p \cos(\omega_p t+\phi_p)+e_g\omega_g \cos(\omega_g t+\phi_g)+\dot{e}_x(t)\right\} \\ -k_m\left\{e_p\sin(\omega_p t+\phi_p)+e_g\sin(\omega_g t+\phi_g)+e_y(t)\right\}-c_{s2}e_g\omega_g\cos(\omega_g t+\phi_g)-k_{s2}e_g\sin(\omega_g t+\phi_g)-m_2 g \end{Bmatrix} \tag{14}$$

where $\mathbf{f}(t)$ is the force vector, and $\mathbf{M}$, $\mathbf{C}$, and $\mathbf{K}$ are the mass, damping, and stiffness symmetric matrices, respectively. Also, m_1 and m_2 are the mass of the pinion and the gear, respectively; k_{s1} and k_{s2} are shaft stiffness for the pinion and the gear, respectively; and c_{s1} and c_{s2} are shaft stiffness for the pinion and the gear, respectively.

This novel approach makes use of existing simple measurement techniques available for the lateral vibration in rotor dynamic systems to validate the system model and identification of asymmetric TE instead of going for expensive torsional vibration measuring equipment, which is not available in hand. Also, it is practically easy to access gear transmission shafts with displacement probes for lateral vibration measurements rather than mounting high-quality encoders to measure the TE of gear mesh by phase demodulation of the pulse signals of encoders as followed in the transitional approach [12].

III. TRANSFORMATION OF EQUATIONS OF MOTION TO FREQUENCY DOMAIN

The force vector, given in equation (14), is simplified after substituting equations (8) and (9). Using complex mathematics as described in Appendix A with Euler's equation, we have equation (15) in the frequency domain with various frequency excitation components as:

$$\begin{aligned} \mathbf{f}_r = &\begin{Bmatrix} S_{1r}+\mathrm{j}S_{1j} \\ S_{2r}+\mathrm{j}S_{2j} \end{Bmatrix}+\begin{Bmatrix} R_{f_{p1r}}+\mathrm{j}R_{f_{p1j}} \\ R_{f_{p2r}}+\mathrm{j}R_{f_{p2j}} \end{Bmatrix}e^{\mathrm{j}\omega_p t}+\begin{Bmatrix} R_{b_{p1r}}+\mathrm{j}R_{b_{p1j}} \\ R_{b_{p2r}}+\mathrm{j}R_{b_{p2j}} \end{Bmatrix}e^{-\mathrm{j}\omega_p t}+\begin{Bmatrix} R_{f_{g1r}}+\mathrm{j}R_{f_{g1j}} \\ R_{f_{g2r}}+\mathrm{j}R_{f_{g2j}} \end{Bmatrix}e^{\mathrm{j}\omega_g t} \\ &+\begin{Bmatrix} R_{b_{g1r}}+\mathrm{j}R_{b_{g1j}} \\ R_{b_{g2r}}+\mathrm{j}R_{b_{g2j}} \end{Bmatrix}e^{-\mathrm{j}\omega_g t}+\sum_{i=1}^{n}\left(\begin{Bmatrix} S_{f_{e1r}}+jS_{f_{e1j}} \\ S_{f_{e2r}}+jS_{f_{e2j}} \end{Bmatrix}e^{j(i\omega_e t)}+\begin{Bmatrix} S_{b_{e1r}}+jS_{b_{e1j}} \\ S_{b_{e2r}}+jS_{b_{e2j}} \end{Bmatrix}e^{-j(i\omega_e t)}\right) \end{aligned} \tag{15}$$

As described in Appendix B, the equations of motion in the frequency domain are grouped into the components of forward and backward whirls. The frequency domain transformation helps in clarifying the whirling features of the gear mesh using its excitation frequency. By combining the static force, the gear mesh force, and the pinion and gear runout/unbalance forces, the equations of motion in the frequency domain using equations (A-63), (A-89), and (A-118) can be written as:

$$\begin{bmatrix} \mathbf{A}_s & \mathbf{0} & \mathbf{0} \\ \mathbf{0} & \mathbf{A}_{fi} & \mathbf{0} \\ \mathbf{0} & \mathbf{0} & \mathbf{A}_{bi} \end{bmatrix}\begin{Bmatrix} \mathbf{p}_s \\ \mathbf{p}_{fi} \\ \mathbf{p}_{bi} \end{Bmatrix}=\begin{Bmatrix} \mathbf{s}_s \\ \mathbf{s}_{fi} \\ \mathbf{s}_{bi} \end{Bmatrix} \tag{16}$$

Herein, i depicts the index of harmonic of gear order, and n depicts a number of harmonics that are assumed in TE. With the presumed value of TE parameters, equation (16) can be used to numerically simulate the transverse vibration response

of a geared-rotor system. Here, we can observe that the equations of motion are linear due to neglect of the torsional vibration coupling. The holistic solutions with assumed parameters of each harmonic should be summed up for $i = 1, 2, 3, \ldots, n$. The full responses can be written in the matrix form by combining the equations for all values of i and are written as:

$$\begin{bmatrix} \mathbf{A}_s & \mathbf{0} & \mathbf{0} & \mathbf{0} & \mathbf{0} & \mathbf{0} & \mathbf{0} \\ & \mathbf{A}_{f1} & \mathbf{0} & \mathbf{0} & \mathbf{0} & \mathbf{0} & \mathbf{0} \\ & & \ddots & \mathbf{0} & \mathbf{0} & \mathbf{0} & \mathbf{0} \\ & & & \mathbf{A}_{fn} & \mathbf{0} & \mathbf{0} & \mathbf{0} \\ & & & & \mathbf{A}_{b1} & \mathbf{0} & \mathbf{0} \\ & & & & & \ddots & \mathbf{0} \\ \text{sym} & & & & & & \mathbf{A}_{bn} \end{bmatrix} \begin{Bmatrix} \mathbf{p}_s \\ \mathbf{p}_{f1} \\ \vdots \\ \mathbf{p}_{fn} \\ \mathbf{p}_{b1} \\ \vdots \\ \mathbf{p}_{bn} \end{Bmatrix} = \begin{Bmatrix} \mathbf{s}_s \\ \mathbf{s}_{f1} \\ \vdots \\ \mathbf{s}_{fn} \\ \mathbf{s}_{b1} \\ \vdots \\ \mathbf{s}_{bn} \end{Bmatrix} \tag{17}$$

This can be put in a simple form for the required number of harmonics as:

$$\mathbf{A}\mathbf{p} = \mathbf{s} \tag{18}$$

The solution of the above equation can be written as:

$$\mathbf{p} = \mathbf{A}^{-1}\mathbf{s} \tag{19}$$

Equation (19) calculates the response function of the forward and backward whirl gear mesh frequencies with an obligatory number of harmonics based on the nature of excitation for known values of all dynamic parameters of the system model. This will be used to test the IA described in the next section.

IV. IDENTIFICATION OF GEAR MESH PARAMETERS

Using the frequency domain formulation discussed in the previous section, it is attempted to identify critical unknown dynamic parameters of gear pair in a three-step estimation process as described below. Figure 2 gives a schematic representation of the step-down IA.

- In the first step, the gear mesh stiffness and the mean TE are estimated using static components of response taken from numerically simulated full-spectrum plots.
- In the second step, gear mesh damping is calculated with the help of estimated gear mesh stiffness and average gearing mass (details of this are given subsequently). Also, variable components of TEs and their initial phases are identified using the gear mesh stiffness estimated from the first step, gear mesh damping and the gear mesh frequency harmonic responses from full-spectrum plots.
- In the third step, the gear runouts and their initial phases are estimated using the estimates of the first and second steps, and responses at the pinion and gear mesh frequencies are taken from full-spectrum plots.

The solution to the identification problem starts with the initial identification of mean TE and gear mesh stiffness using static response components. For this purpose, static displacement coefficients from the frequency domain formulation, given in Appendix A, equations (A-61) and (A-62) are combined in the matrix form as:

$$\begin{Bmatrix} S_{1r} \\ S_{1j} \\ S_{2r} \\ S_{2j} \end{Bmatrix} = \begin{Bmatrix} k_{s1}P_{s1r} + k_m(P_{s1r} - P_{s2r}) \\ k_{s1}P_{s1j} + k_m(P_{s1j} - P_{s2j}) \\ k_{s2}P_{s2r} + k_m(P_{s2r} - P_{s1r}) \\ k_{s2}P_{s2j} + k_m(P_{s2j} - P_{s1j}) \end{Bmatrix} \tag{20}$$

by substituting equation (A-41) into equation (20) and unknown terms are rearranged as:

$$\begin{Bmatrix} k_m e_m \\ k_m e_m \\ k_m e_m \\ k_m e_m \end{Bmatrix} = \begin{Bmatrix} k_{s1}P_{s1r} + k_m(P_{s1r} - P_{s2r}) \\ k_{s1}P_{s1j} + k_m(P_{s1j} - P_{s2j}) + m_1 g \\ -k_{s2}P_{s2r} - k_m(P_{s2r} - P_{s1r}) \\ -k_{s2}P_{s2j} - k_m(P_{s2j} - P_{s1j}) - m_2 g \end{Bmatrix} \tag{21}$$

The gear mesh stiffness and mean TE are separated and written in matrix form as:

$$\begin{bmatrix} (P_{1r} - P_{2r}) & -1 \\ (P_{1j} - P_{2j}) & -1 \\ (P_{2r} - P_{1r}) & 1 \\ (P_{2j} - P_{1j}) & 1 \end{bmatrix} \begin{Bmatrix} k_m \\ k_m e_m \end{Bmatrix} = \begin{Bmatrix} -k_{s1}P_{1r} \\ -k_{s1}P_{1j} - m_1 g \\ -k_{s2}P_{2r} \\ -k_{s2}P_{2j} - m_2 g \end{Bmatrix} \tag{22}$$

In the first step of the identification problem, the gear mesh stiffness (k_m) and the mean TE (e_m) are estimated

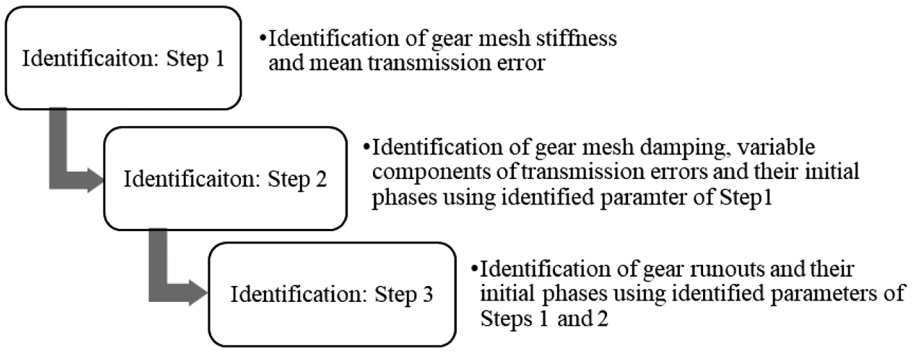

Fig. 2. Schematic representation of identification algorithm step-down process.

using the static response (P) terms. On the left and right sides of the matrix in equation (22), the P terms are taken from full-spectrum plots. On pseudo-inverting the first (left) matrix in equation (22) we get k_m and e_m.

In the second step of the identification process, the gear mesh frequency components are considered for the identification of the gear mesh damping and variable TE with its magnitudes and initial phases. For this purpose, equations (A-20), (A-22), (A-24), and (A-26) are grouped as:

$$\begin{Bmatrix} R_{f_e r} \\ R_{f_e j} \\ R_{b_e r} \\ R_{b_e j} \end{Bmatrix} = \begin{Bmatrix} e_{xi}\cos\phi_{e_{xi}} - e_{yi}sin\phi_{e_{yi}} \\ e_{xi}sin\phi_{e_{xi}} + e_{yi}\cos\phi_{e_{yi}} \\ e_{xi}\cos\phi_{e_{xi}} + e_{yi}\sin\phi_{e_{yi}} \\ -e_{xi}\sin\phi_{e_{xi}} + e_{yi}\cos\phi_{e_{yi}} \end{Bmatrix} \Rightarrow \begin{bmatrix} 1 & -1 & 0 & 0 \\ 0 & 0 & 1 & 1 \\ 1 & 1 & 0 & 0 \\ 0 & 0 & -1 & 1 \end{bmatrix} \begin{Bmatrix} e_{xi}\cos\phi_{e_{xi}} \\ e_{yi}sin\phi_{e_{yi}} \\ e_{xi}sin\phi_{e_{xi}} \\ e_{yi}\cos\phi_{e_{yi}} \end{Bmatrix} = \{T\} \tag{23}$$

Now, the forcing functions due to gear mesh frequency on the input and output shafts are grouped for the input shaft by substituting these equations in equations (A-42) and (A-43) to get the defined pinion and gear force real and imaginary components ® in terms of critical gear mesh parameters on the input shaft as:

$$\begin{Bmatrix} S_{f_{e1r}} \\ S_{f_{e1j}} \\ S_{b_{e1r}} \\ S_{b_{e1j}} \end{Bmatrix} = \frac{1}{2}\begin{bmatrix} i\omega_e c_m & k_m & 0 & 0 \\ -k_m & i\omega_e c_m & 0 & 0 \\ 0 & 0 & i\omega_e c_m & -k_m \\ 0 & 0 & k_m & i\omega_e c_m \end{bmatrix} \begin{bmatrix} 1 & -1 & 0 & 0 \\ 0 & 0 & 1 & 1 \\ 1 & 1 & 0 & 0 \\ 0 & 0 & -1 & 1 \end{bmatrix} \begin{Bmatrix} e_{xi}\cos\phi_{e_{xi}} \\ e_{yi}sin\phi_{e_{yi}} \\ e_{xi}sin\phi_{e_{xi}} \\ e_{yi}\cos\phi_{e_{yi}} \end{Bmatrix}$$
$$\Rightarrow \frac{1}{2}\begin{bmatrix} i\omega_e c_m & -i\omega_e c_m & k_m & k_m \\ -k_m & k_m & i\omega_e c_m & i\omega_e c_m \\ i\omega_e c_m & i\omega_e c_m & k_m & -k_m \\ k_m & k_m & -i\omega_e c_m & i\omega_e c_m \end{bmatrix} \begin{Bmatrix} e_{xi}\cos\phi_{e_{xi}} \\ e_{yi}sin\phi_{e_{yi}} \\ e_{xi}sin\phi_{e_{xi}} \\ e_{yi}\cos\phi_{e_{yi}} \end{Bmatrix} \tag{24}$$

Similarly, for the output shaft, we can write as:

$$\begin{Bmatrix} S_{f_{e2r}} \\ S_{f_{e2j}} \\ S_{b_{e2r}} \\ S_{b_{e2j}} \end{Bmatrix} = \frac{1}{2}\begin{bmatrix} -i\omega_e c_m & -k_m & 0 & 0 \\ k_m & -i\omega_e c_m & 0 & 0 \\ 0 & 0 & -i\omega_e c_m & k_m \\ 0 & 0 & -k_m & -i\omega_e c_m \end{bmatrix} \begin{bmatrix} 1 & -1 & 0 & 0 \\ 0 & 0 & 1 & 1 \\ 1 & 1 & 0 & 0 \\ 0 & 0 & -1 & 1 \end{bmatrix} \begin{Bmatrix} e_{xi}\cos\phi_{e_{xi}} \\ e_{yi}sin\phi_{e_{yi}} \\ e_{xi}sin\phi_{e_{xi}} \\ e_{yi}\cos\phi_{e_{yi}} \end{Bmatrix}$$
$$\Rightarrow \frac{1}{2}\begin{bmatrix} -i\omega_e c_m & i\omega_e c_m & -k_m & -k_m \\ k_m & -k_m & -i\omega_e c_m & -i\omega_e c_m \\ -i\omega_e c_m & -i\omega_e c_m & -k_m & k_m \\ -k_m & -k_m & i\omega_e c_m & -i\omega_e c_m \end{bmatrix} \begin{Bmatrix} e_{xi}\cos\phi_{e_{xi}} \\ e_{yi}sin\phi_{e_{yi}} \\ e_{xi}sin\phi_{e_{xi}} \\ e_{yi}\cos\phi_{e_{yi}} \end{Bmatrix} \tag{25}$$

These equation formulations are used for the second step of identification by substituting them into equations (A-77), (A-80), (A-83), (A-86), (A-106), (A-109), (A-112), and (A-115) to get the identification equations of the input and output shafts.

These equations are written in the matrix form by rearranging terms for the input shaft as:

$$\frac{1}{2}\begin{bmatrix} i\omega_e c_m & -i\omega_e c_m & k_m & k_m \\ -k_m & k_m & i\omega_e c_m & i\omega_e c_m \\ i\omega_e c_m & i\omega_e c_m & k_m & -k_m \\ k_m & k_m & -i\omega_e c_m & i\omega_e c_m \end{bmatrix} \begin{Bmatrix} e_{xi}\cos\phi_{e_{xi}} \\ e_{yi}sin\phi_{e_{yi}} \\ e_{xi}sin\phi_{e_{xi}} \\ e_{yi}\cos\phi_{e_{yi}} \end{Bmatrix}$$
$$= \begin{Bmatrix} -m_1(i\omega_e)^2 P_{f_e 1r} - (i\omega_e)c_{s1}P_{f_e 1j} + k_{s1}P_{f_e 1r} + k_m(P_{f_e 1r} - P_{f_e 2r}) - (i\omega_e c_m)(P_{f_e 1j} - P_{f_e 2j}) \\ -m_1(i\omega_e)^2 P_{f_e 1j} + i\omega_e c_{s1}P_{f_e 1r} + k_{s1}P_{f_e 1j} + k_m(P_{f_e 1j} - P_{f_e 2j}) + i\omega_e c_m(P_{f_e 1r} - P_{f_e 2r}) \\ -m_1(i\omega_e)^2 P_{b_e 1r} + i\omega_e c_{s1}P_{b_e 1j} + k_{s1}P_{b_e 1r} + k_m(P_{b_e 1r} - P_{b_e 2r}) + (i\omega_e c_m)(P_{b_e 1j} - P_{b_e 2j}) \\ -m_1(i\omega_e)^2 P_{b_e 1j} - i\omega_e c_{s1}P_{b_e 1r} + k_{s1}P_{b_e 1j} + k_m(P_{b_e 1j} - P_{b_e 2j}) + i\omega_e c_m(P_{b_e 2r} - P_{b_e 1r}) \end{Bmatrix} \tag{26}$$

Similarly, for the output shaft, it can be arranged as:

$$\frac{1}{2}\begin{bmatrix} -i\omega_e c_m & i\omega_e c_m & -k_m & -k_m \\ k_m & -k_m & -i\omega_e c_m & -i\omega_e c_m \\ -i\omega_e c_m & -i\omega_e c_m & -k_m & k_m \\ -k_m & -k_m & i\omega_e c_m & -i\omega_e c_m \end{bmatrix} \begin{Bmatrix} e_{xi}\cos\phi_{e_{xi}} \\ e_{yi}sin\phi_{e_{yi}} \\ e_{xi}sin\phi_{e_{xi}} \\ e_{yi}\cos\phi_{e_{yi}} \end{Bmatrix}$$
$$= \begin{Bmatrix} -m_2(i\omega_e)^2 P_{f_e 2r} - i\omega_e c_{s2} P_{f_e 2j} + k_{s2} P_{f_e 2r} + k_m(P_{f_e 2r} - P_{f_e 1r}) + i\omega_e c_m(P_{f_e 1j} - P_{f_e 2j}) \\ -m_2(i\omega_e)^2 P_{f_e 2j} + i\omega_e c_{s2} P_{f_e 2r} + k_{s2} P_{f_e 2j} + k_m(P_{f_e 2j} - P_{f_e 1j}) + i\omega_e c_m(P_{f_e 2r} - P_{f_e 1r}) \\ -m_2(i\omega_e)^2 P_{b_e 2r} + i\omega_e c_{s2} P_{b_e 2j} + k_{s2} P_{b_e 2r} + k_m(P_{b_e 2r} - P_{b_e 1r}) + i\omega_e c_m(P_{b_e 2j} - P_{b_e 1j}) \\ -m_2(i\omega_e)^2 P_{b_e 2j} - i\omega_e c_{s2} P_{b_e 2r} + k_{s2} P_{b_e 2j} + k_m(P_{b_e 2j} - P_{b_e 1j}) + i\omega_e c_m(P_{b_e 1r} - P_{b_e 2r}) \end{Bmatrix} \tag{27}$$

Herein, the gear mesh damping is estimated from gear mesh stiffness, k_m, and average pinion (m_p) and gear (m_g) masses. The average mass of pinion and gear is given by average gearing mass as:

$$m_{avg} = \frac{m_p m_g}{m_p + m_g} \tag{28}$$

The gear mesh damping can be calculated using the free vibration damping formula with average gearing mass and gear mesh stiffness by using an assumed gear mesh damping ratio (ζ_m) value of 0.01 as:

$$c_m = 2\zeta_m \sqrt{k_m m_{avg}} \tag{29}$$

equations (26) and (27) are combined in the matrix form as:

$$\frac{1}{2}\begin{bmatrix} i\omega_e c_m & -i\omega_e c_m & k_m & k_m \\ -k_m & k_m & i\omega_e c_m & i\omega_e c_m \\ i\omega_e c_m & i\omega_e c_m & k_m & -k_m \\ k_m & k_m & -i\omega_e c_m & i\omega_e c_m \\ -i\omega_e c_m & i\omega_e c_m & -k_m & -k_m \\ k_m & -k_m & -i\omega_e c_m & -i\omega_e c_m \\ -i\omega_e c_m & -i\omega_e c_m & -k_m & k_m \\ -k_m & -k_m & i\omega_e c_m & -i\omega_e c_m \end{bmatrix} \begin{Bmatrix} e_{xi}\cos\phi_{e_{xi}} \\ e_{yi}sin\phi_{e_{yi}} \\ e_{xi}sin\phi_{e_{xi}} \\ e_{yi}\cos\phi_{e_{yi}} \end{Bmatrix}$$
$$= \begin{Bmatrix} -m_1(i\omega_e)^2 P_{f_e 1r} - (i\omega_e)c_{s1} P_{f_e 1j} + k_{s1} P_{f_e 1r} + k_m(P_{f_e 1r} - P_{f_e 2r}) - (i\omega_e c_m)(P_{f_e 1j} - P_{f_e 2j}) \\ -m_1(i\omega_e)^2 P_{f_e 1j} + i\omega_e c_{s1} P_{f_e 1r} + k_{s1} P_{f_e 1j} + k_m(P_{f_e 1j} - P_{f_e 2j}) + i\omega_e c_m(P_{f_e 1r} - P_{f_e 2r}) \\ -m_1(i\omega_e)^2 P_{b_e 1r} + i\omega_e c_{s1} P_{b_e 1j} + k_{s1} P_{b_e 1r} + k_m(P_{b_e 1r} - P_{b_e 2r}) + (i\omega_e c_m)(P_{b_e 1j} - P_{b_e 2j}) \\ -m_1(i\omega_e)^2 P_{b_e 1j} - i\omega_e c_{s1} P_{b_e 1r} + k_{s1} P_{b_e 1j} + k_m(P_{b_e 1j} - P_{b_e 2j}) + i\omega_e c_m(P_{b_e 2r} - P_{b_e 1r}) \\ -m_2(i\omega_e)^2 P_{f_e 2r} - i\omega_e c_{s2} P_{f_e 2j} + k_{s2} P_{f_e 2r} + k_m(P_{f_e 2r} - P_{f_e 1r}) + i\omega_e c_m(P_{f_e 1j} - P_{f_e 2j}) \\ -m_2(i\omega_e)^2 P_{f_e 2j} + i\omega_e c_{s2} P_{f_e 2r} + k_{s2} P_{f_e 2j} + k_m(P_{f_e 2j} - P_{f_e 1j}) + i\omega_e c_m(P_{f_e 2r} - P_{f_e 1r}) \\ -m_2(i\omega_e)^2 P_{b_e 2r} + i\omega_e c_{s2} P_{b_e 2j} + k_{s2} P_{b_e 2r} + k_m(P_{b_e 2r} - P_{b_e 1r}) + i\omega_e c_m(P_{b_e 2j} - P_{b_e 1j}) \\ -m_2(i\omega_e)^2 P_{b_e 2j} - i\omega_e c_{s2} P_{b_e 2r} + k_{s2} P_{b_e 2j} + k_m(P_{b_e 2j} - P_{b_e 1j}) + i\omega_e c_m(P_{b_e 1r} - P_{b_e 2r}) \end{Bmatrix} \tag{30}$$

Herein, subscripts 1 and 2 represent the input and output shafts. The harmonic number i is from 1 to 5 harmonics of gear mesh frequencies considered in modeling variable TE, the gear mesh damping from equation (29), the gear mesh stiffness calculated from Step 1, the input and output shaft stiffness, the masses of gears, and the full-spectrum responses (P terms) calculated numerically are substituted in equation (30). On taking the pseudo-inverse of the regression equation (30) to identify the four unknown quantities of fluctuating part of TE and their phases are written as:

$$\begin{Bmatrix} e_{fxi}\cos\phi_{e_{xi}} \\ e_{fyi}sin\phi_{e_{yi}} \\ e_{fxi}sin\phi_{e_{xi}} \\ e_{fyi}\cos\phi_{e_{yi}} \end{Bmatrix} = \begin{Bmatrix} e_{11} \\ e_{21} \\ e_{31} \\ e_{41} \end{Bmatrix} \tag{31}$$

On noting equation (31), the fluctuating part of the static TE in the x and y directions are estimated using the sine and cosine trigonometric relations by combining the first and third components and then by combining the second and fourth components as:

$$e_{fxi} = \sqrt{e_{11}^2 + e_{31}^2}; \quad e_{fyi} = \sqrt{e_{21}^2 + e_{41}^2} \tag{32}$$

From the first and second components of equation (31), we get the initial phases of fluctuating components of the static TE in the x and y directions which are estimated as:

$$\phi_{e_{xi}} = \cos^{-1}(e_{11}/e_{xi}); \quad \phi_{e_{yi}} = \sin^{-1}(e_{21}/e_{yi}) \tag{33}$$

In the third and last step, the gear runouts and their phases are identified with the pinion and gear mesh frequency components of frequency domain transformations. The defined pinion and gear force real and imaginary components (R) in equations (A-30) through (A-33), (A-35), (A-36), (A-38), and (A-39) are substituted into equations (A-107), (A-113), (A-110), (A-116), (A-79), (A-85), (A-81), and (A-88), respectively, to get the identification equations on the input and output shafts for the *i*th harmonic and are written in the matrix form by rearranging pinion equations as:

$$\begin{bmatrix} (m_1\omega_p^2 - k_m - k_{s1}) & (c_m\omega_p + c_{s1}\omega_p) & 0 & 0 \\ (c_m\omega_p + c_{s1}\omega_p) & (-m_1\omega_p^2 + k_m + k_{s1}) & 0 & 0 \\ k_m & -c_m\omega_p & 0 & 0 \\ -c_m\omega_p & -k_m & 0 & 0 \end{bmatrix} \begin{Bmatrix} e_p\cos\varphi_p \\ e_p\sin\varphi_p \\ e_g\cos\varphi_g \\ e_g\sin\varphi_g \end{Bmatrix}$$

$$= \begin{bmatrix} -m_1(i\omega_p)^2 P_{b_{p1r}} + i\omega_p c_{s1} P_{b_{p1j}} + k_{s1} P_{b_{p1r}} + k_m(P_{b_{p1r}} - P_{b_{p2r}}) + i\omega_p c_m(P_{b_{p1j}} - P_{b_{p2j}}) \\ -m_1(i\omega_p)^2 P_{b_{p1j}} - i\omega_p c_{s1} P_{b_{p1r}} + k_{s1} P_{b_{p1j}} + k_m(P_{b_{p1j}} - P_{b_{p2j}}) + i\omega_p c_m(P_{b_{p2r}} - P_{b_{p1r}}) \\ m_2(i\omega_p)^2 P_{b_{p2r}} - i\omega_p c_{s2} P_{b_{p2j}} - k_{s2} P_{b_{p2r}} - k_m(P_{b_{p2r}} - P_{b_{p1r}}) - i\omega_p c_m(P_{b_{p2j}} - P_{b_{p1j}}) \\ m_2(i\omega_p)^2 P_{b_{p2j}} + i\omega_p c_{s2} P_{b_{p2j}} - k_{s2} P_{b_{p2j}} - k_m(P_{b_{p2j}} - P_{b_{p1j}}) - i\omega_p c_m(P_{b_{p1r}} - P_{b_{p2r}}) \end{bmatrix} \tag{34}$$

and gear equations as:

$$\begin{bmatrix} 0 & 0 & k_m & -c_m\omega_g \\ 0 & 0 & c_m\omega_g & k_m \\ 0 & 0 & m_2\omega_g^2 - k_m - k_{s2} & c_m\omega_g + c_{s2}\omega_g \\ 0 & 0 & -(c_m\omega_g + c_{s2}\omega_g) & m_2\omega_g^2 - k_m - k_{s2} \end{bmatrix} \begin{Bmatrix} e_p\cos\varphi_p \\ e_p\sin\varphi_p \\ e_g\cos\varphi_g \\ e_g\sin\varphi_g \end{Bmatrix}$$

$$= \begin{bmatrix} -m_1(i\omega_g)^2 P_{f_{g1r}} - i\omega_g c_{s1} P_{f_{g1j}} + k_{s1} P_{f_{g1r}} + k_m(P_{f_{g1r}} - P_{f_{g2r}}) - i\omega_g c_m(P_{f_{g1j}} - P_{f_{g2j}}) \\ -m_1(i\omega_g)^2 P_{f_{g1j}} + i\omega_g c_{s1} P_{f_{g1r}} + k_{s1} P_{f_{g1j}} + k_m(P_{f_g1j} - P_{f_{g2j}}) + i\omega_g c_m(P_{f_{g1r}} - P_{f_{g2r}}) \\ m_2(i\omega_g)^2 P_{f_{g2r}} + i\omega_g c_{s2} P_{f_{g2j}} - k_{s2} P_{f_{g2r}} - k_m(P_{f_{g2r}} - P_{f_{g1r}}) + i\omega_g c_m(P_{f_{g2j}} - P_{f_{g1j}}) \\ m_2(i\omega_g)^2 P_{f_{g2j}} - i\omega_g c_{s2} P_{f_{g2r}} - k_{s2} P_{f_{g2j}} - k_m(P_{f_{g1r}} - P_{f_{g2r}}) - i\omega_g c_m(P_{f_{g2r}} - P_{f_{g1r}}) \end{bmatrix} \tag{35}$$

By substituting the identified value of gear mesh stiffness (k_m) and gear mesh damping (c_m) from the first and second steps, chosen geared-rotor parameters given in Table I and full-spectrum amplitudes at respective harmonics (P terms) in equations (27) and (28) and resulting equations are simplified to get the combined form as:

$$\begin{bmatrix} m_1\omega_p^2 - k_m - k_{s1} & c_m\omega_p + c_{s1}\omega_p & 0 & 0 \\ c_m\omega_p + c_{s1}\omega_p & -m_1\omega_p^2 + k_m + k_{s1} & 0 & 0 \\ k_m & -c_m\omega_p & 0 & 0 \\ -c_m\omega_p & -k_m & 0 & 0 \\ 0 & 0 & k_m & -c_m\omega_g \\ 0 & 0 & c_m\omega_g & k_m \\ 0 & 0 & m_2\omega_g^2 - k_m - k_{s2} & c_m\omega_g + c_{s2}\omega_g \\ 0 & 0 & -c_m\omega_g - c_{s2}\omega_g & m_2\omega_g^2 - k_m - k_{s2} \end{bmatrix} \begin{Bmatrix} e_p\cos\varphi_p \\ e_p\sin\varphi_p \\ e_g\cos\varphi_g \\ e_g\sin\varphi_g \end{Bmatrix}$$

$$= \begin{bmatrix} -m_1(\omega_p)^2 P_{b_{p1r}} + i\omega_p c_{s1} P_{b_{p1j}} + k_{s1} P_{b_{p1r}} + k_m(P_{b_{p1r}} - P_{b_{p2r}}) + i\omega_p c_m(P_{b_{p1j}} - P_{b_{p2j}}) \\ -m_1(\omega_p)^2 P_{b_{p1j}} - i\omega_p c_{s1} P_{b_{p1r}} + k_{s1} P_{b_{p1j}} + k_m(P_{b_{p1j}} - P_{b_{p2j}}) + i\omega_p c_m(P_{b_{p2r}} - P_{b_{p1r}}) \\ -m_2(\omega_p)^2 P_{b_{p2r}} + i\omega_p c_{s2} P_{b_{p2j}} + k_{s2} P_{b_{p2r}} + k_m(P_{b_{p2r}} - P_{b_{p1r}}) + i\omega_p c_m(P_{b_{p2j}} - P_{b_{p1j}}) \\ -m_2(\omega_p)^2 P_{b_{p2j}} - i\omega_p c_{s2} P_{b_{p2r}} + k_{s2} P_{b_{p2j}} + k_m(P_{b_{p2j}} - P_{b_{p1j}}) + i\omega_p c_m(P_{b_{p1r}} - P_{b_{p2r}}) \\ -m_1(\omega_g)^2 P_{f_{g1r}} - i\omega_g c_{s1} P_{f_{g1j}} + k_{s1} P_{f_{g1r}} + k_m(P_{f_{g1r}} - P_{f_{g2r}}) - i\omega_g c_m(P_{f_{g1j}} - P_{f_{g2j}}) \\ -m_1(\omega_g)^2 P_{f_{g1j}} + i\omega_g c_{s1} P_{f_{g1r}} + k_{s1} P_{f_{g1j}} + k_m(P_{f_g1j} - P_{f_{g2j}}) + i\omega_g c_m(P_{f_{g1r}} - P_{f_{g2r}}) \\ -m_2(\omega_g)^2 P_{f_{g2r}} - i\omega_g c_{s2} P_{f_{g2j}} + k_{s2} P_{f_{g2r}} + k_m(P_{f_{g2r}} - P_{f_{g1r}}) + i\omega_g c_m(P_{f_{g2j}} - P_{f_{g1j}}) \\ -m_2(\omega_g)^2 P_{f_{g2j}} + i\omega_g c_{s2} P_{f_{g2r}} + k_{s2} P_{f_{g2j}} + k_m(P_{f_{g2j}} - P_{f_{g1j}}) + i\omega_g c_m(P_{f_{g2r}} - P_{f_{g1r}}) \end{bmatrix} \tag{36}$$

In the third step of the identification problem, the matrix in equation (36) is pseudo-inverted using the regression fit for identifying the pinion and gear runouts. The resulting form of the vector is written as:

Table I. Gear mesh vibration problem assumptions

Item	Measure	Worth
Radius of shafts	Meter	0.0055
Shafts damping ratio	No units	0.01
Length of shafts	Meter	0.190
Drive gear mass	Kilogram	0.310
Output shaft gear mass	Kilogram	1.270
Count of driven gear tooth	No units	35
Count of drive gear tooth	No units	16
Driving gear RPM	RPM	660.0
Torque of driven shaft	N-m	0.110
Modulus of elasticity of shafts	M Pa	2×10^5
Stiffness of shafts	N/m	1×10^6
Stiffness of gear mesh	N/m	6×10^8
Gear mesh damping ratio	No units	0.02
Gear mesh mass	Kilogram	0.3010
Gear mesh damping	Ns/m	77.780
Number of harmonics	No units	5
Mean TE	Micron	50
Gravitational acceleration	m/s^2	9.81
Fluctuating TE in x (harmonics of peak-to-peak TE)	Micron	e_{rx1} 40
		e_{rx2} 25
		e_{rx3} 35
		e_{rx4} 20
		e_{rx5} 10
Phase of TE in x	Radian	0.785
Fluctuating TE in y (harmonics of peak-to-peak TE)	Micron	e_{ry1} 30
		e_{ry2} 15
		e_{ry3} 25
		e_{ry4} 10
		e_{ry5} 5
Phase of TE in y	Radian	1.570
Pinion runout	Micron	200
Gear runout	Micron	300
Phase of pinion runout	Radian	1.047
Phase of gear runout	Radian	2.094

$$\begin{Bmatrix} e_p\cos\varphi_p \\ e_p\sin\varphi_p \\ e_g\cos\varphi_g \\ e_g\sin\varphi_g \end{Bmatrix} = \begin{Bmatrix} e_{p1} \\ e_{p2} \\ e_{g1} \\ e_{g2} \end{Bmatrix} \tag{37}$$

On noting equation (37), the pinion and gear runouts are estimated using the sine and cosine trigonometric relations by combining the first and second components and then by combining the third and fourth components as:

$$e_p = \sqrt{e_{p1}^2 + e_{p2}^2}; \quad e_g = \sqrt{e_{g1}^2 + e_{g2}^2} \tag{38}$$

From the first and second components of equation (37), we get the initial phases of the pinion and gear runout frequencies which are estimated as:

$$\phi_{e_p} = \cos^{-1}(e_{p1}/e_p); \quad \phi_{e_g} = \cos^{-1}(e_{g1}/e_g) \tag{39}$$

With this three-step process, the estimation of all eleven-gear mesh DTE parameters that influence the lateral responses of the spur geared-rotor system with parallel shafts has been presented. Now through numerical simulation, the displacement responses are generated and analyzed for chosen system parameters. These responses will be used to evaluate the proposed IA to get the estimation of the chosen system parameters.

V. GEARED-ROTOR RESPONSE NUMERICAL SIMULATION

The equations of motion of geared-rotor system are solved numerically using the Runge–Kutta technique in MATLAB with function *ode45* for time domain solution. Traditionally, the transformation of the calculated solution into frequency domain FFT gives information about various frequency components existing in the vibration spectrum. It contains both magnitude and phase information of response to analyze the system dynamics. However, the response spectrum does not indicate about relative phase direction among different vibration signals. In addition, it fails to provide the direction of the pinon and gear harmonics with respect to the direction of the drive shaft.

The geared-rotor vibration signals in the x and y directions are plotted for two transverse directions to get orbit. It may include multiple components of the forward and backward whirls. Both magnitude and phase of various frequency components are required to get the actual shape of the rotor orbit. Full-spectrum plot is a convenient tool to identify whether the orbit at a frequency component is of forward or backward whirl with respect to rotor spin direction [26]. Rao and Tiwari [45] analyzed geared-rotor response to detect qualitatively the asymmetric TE using a full-spectrum plot. Relative phase correlation of two vibration signals was used in a full-spectrum plot to split the geared-rotor frequency into the forward (positive) whirl frequency component and backward (negative) whirl frequency component, which constitute the orbit. For gears due to asymmetric TE, the forward and backward whirls come into existence, and with conventional FFT methods this asymmetry cannot be found. In conventional FFT methods, both forward and backward whirls overlap at the same frequency.

Displacement responses are calculated in the time domain using linear differential equations of motion using geared-rotor data given in Table I. Figure 3 shows the orbit plot using numerically calculated time domain response. Different orbit shapes for the input and output shafts are attributed to different parameters chosen for the pinion and the gear. Figure 4 shows the full-spectrum response in the form of Bode plots calculated using *fftshift* function of MATLAB applied on the numerically calculated time domain response. The response displays the features of a grouping of multiple harmonics. The five harmonics 176, 352, 528, 704, and 880 Hz are manifested in the full-spectrum response in the forward and backward whirl frequencies, of which the initial three harmonics are dominant and the rest of the two are minor due to the assumed lower TE at higher harmonics. The phase shift is also observed at each of the harmonic in Fig. 4 for both input and output shaft responses. The utility of full-spectrum response is to analyze the whirl amplitudes of different harmonics present in the gear drive due to the TE.

The impact of measurement noise is analyzed using numerically generated response by mixing 5% Gaussian

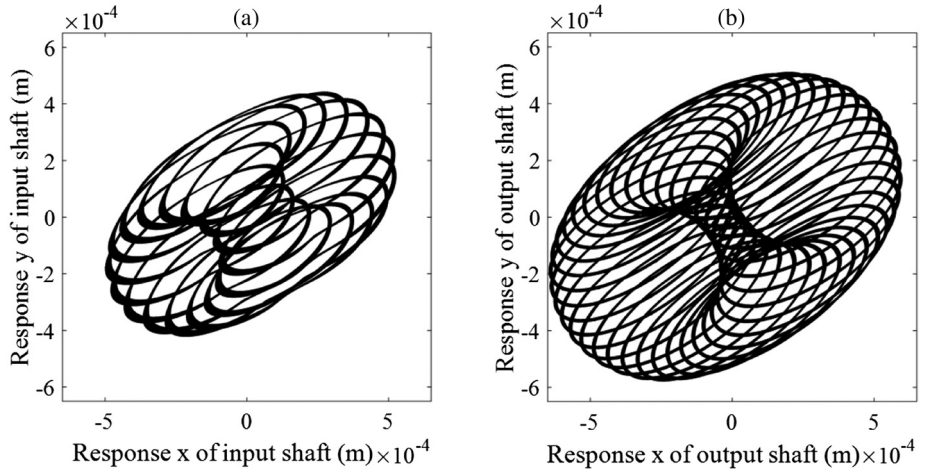

Fig. 3. (a) Orbit plot of the drive shaft; (b) orbit plot of the driven shaft.

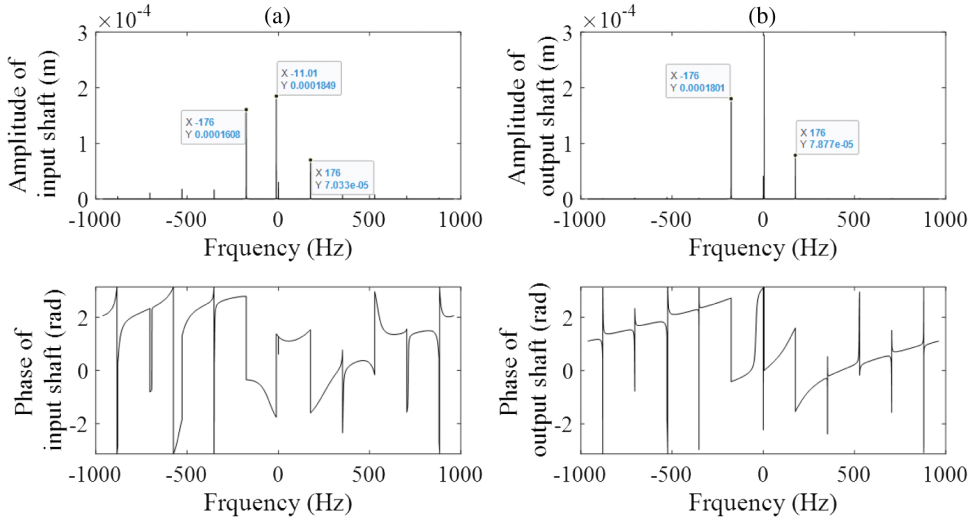

Fig. 4. (a) Full-spectrum Bode plot of drive shaft; (b) full-spectrum Bode plot of driven shaft.

white noise into signal in timescale. Full-spectrum plot in Fig. 5 with measurement noise shows that the noise has hardly any effect on the response in the frequency range of analysis.

VI. NUMERICAL TESTING OF IA

To test the three-step IA described in Section IV, estimation of TE parameters is performed using numerically generated full-spectrum responses (P terms, which are real and imaginary components of full-spectrum amplitudes) as shown in Fig. 4(a) and 4(b) where magnitudes of the real and imaginary components are shown for the first harmonic of gear mesh frequency. Since the present IA is based on linear least-squares fit, the algorithm is not dependent on initial guest and no iteration is involved. For improving the conditioning of matrix, suitable scaling has been done.

The estimates are compared with parameters chosen for simulating numerical responses as given in Table II. The percentage deviation of the estimates with assumed parameters for numerical simulation is also presented. It is observed that the proposed IA estimates are perfectly matching with the assumed values without any deviation. Also, the estimations are checked by changing the harmonic number from 1 to 5. For all five harmonics, the estimates are perfectly matching with assumed variables.

To test the robustness of the proposed IA against noise present in measurement data, 1 % and 5 % white Gaussian noise is introduced in the numerically simulated data. The full-spectrum response is plotted with 5 % Gaussian noise, as shown in Fig. 6, in the amplitude and phase form (Bode plot), and is used for the identification purpose. The comparison of phase between these two plots, Figs. 4 and 6, shows the effect of adding 5% Gaussian measurement noise with quickly varying phase in the entire spectrum in Fig. 6.

With the same identification procedure used without noise case, the estimates are calculated with measurement noise in the full-spectrum response by increasing from 1% up to 5% serially. It is observed that with noise the estimates of gear mesh stiffness and mean TE are deviating. Table II shows the percent deviations of estimates with noise and without noise for varied presumed gear mesh parameters by changing the shaft speed, gear mesh stiffness, mean TE,

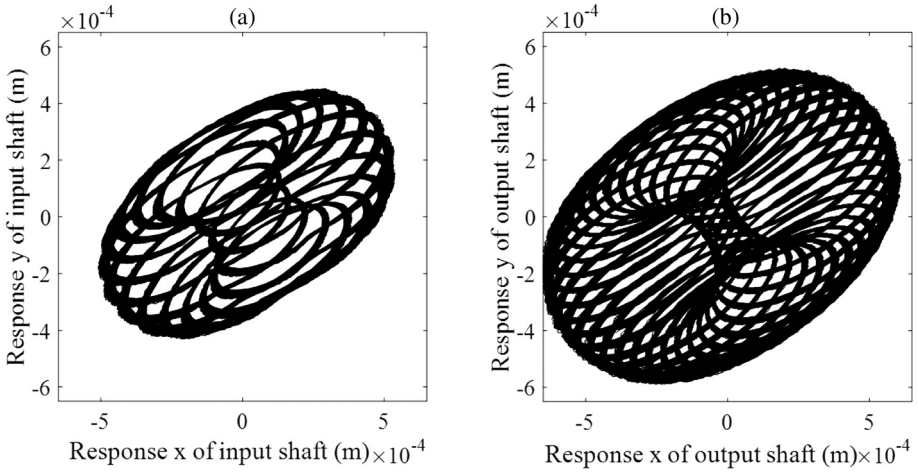

Fig. 5. (a) Orbit response plot of input shaft with noise; (b) orbit response plot of output shaft with noise.

variable TE, gear runouts, and damping. It is observed that without considering measurement noise, the identified estimates are perfectly matching with presumed parameters used in numerical simulations, as shown in Table II, for the first harmonic.

Table II shows the percent deviation in the estimates with the increase in measurement noise mainly due to deviation in gear mesh stiffness and slight deviation in mesh TE in all cases, which is sensitive to static deflection. Also, it is observed that without passing the deviated gear mesh stiffness and the mean TE due to measurement noise in the second and third steps of IA, the estimates of TE and runout parameters are robust to the measurement noise. To avoid these deviations, one may calculate gear mesh stiffness using the Hertzian contact formulation presented in Flek *et al.* [37] analytically or by the FE model.

Table II. Identification summary based on numerical simulation of first harmonic

Varied parameter		Percentage deviation of identified parameter with assumed one (%)										
Following parameters are varied to check the robustness of IA		k_m	e_m	c_m	$e_{fxi}(t)$	$e_{fyi}(t)$	ϕ_{exi}	ϕ_{eyi}	e_p	e_g	ϕ_p	ϕ_g
Noise	Speed (RPM)											
0	660	0	0	0	0	0	0	0	0	0	0	0
0	1320	0	0	0	0	0	0	0	0	0	0	0
1	660	–96	1.8	0	–12	–14	13	–5	0.2	0.1	–0.1	0.04
5	660	–99	10	0	–4.1	–16	103	–52	1.1	0.7	–0.6	0.2
Noise	Gear mesh stiffness (N/m)											
0	6e8	0	0	0	0	0	0	0	0	0	0	0
0	7e8	0	0	0	0	0	0	0	0	0	0	0
5	6e8	–99	10	0	–4.1	–16	103	–52	1.1	0.7	–0.6	0.2
Noise	Mean TE (μm)											
0	10	0	0	0	0	0	0	0	0	0	0	0
0	100	0	0	0	0	0	0	0	0	0	0	0
5	10	–99	10	0	–4.1	–16	103	–52	1.1	0.7	–0.6	0.2
Noise	Variable TE (μm)											
0	10	0	0	0	0	0	0	0	0	0	0	0
0	50	0	0	0	0	0	0	0	0	0	0	0
5	10	–99	10	0	–4.1	–16	103	–52	1.1	0.7	–0.6	0.2
Noise	Runouts (μm)											
0	100	0	0	0	0	0	0	0	0	0	0	0
0	200	0	0	0	0	0	0	0	0	0	0	0
5	100	–99	10	0	–4.1	–16	103	–52	1.1	0.7	–0.6	0.2
Noise	Damping											
0	0.01	0	0	0	0	0	0	0	0	0	0	0
0	0.02	0	0	0	0	0	0	0	0	0	0	0
5	0.01	–99	10	0	–4.1	–16	103	–52	1.1	0.7	–0.6	0.2

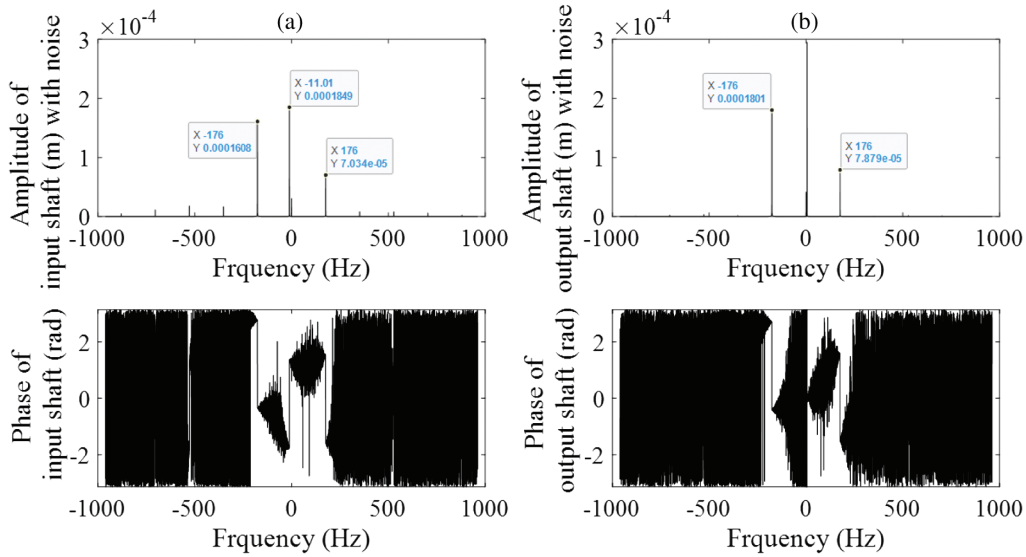

Fig. 6. (a) Full-spectrum Bode plot of drive shaft when noise is introduced; (b) full-spectrum Bode plot of driven shaft when noise is introduced.

Table III. Identification summary with noise and higher harmonics

Varied parameter		Percentage deviation of identified parameter with assumed one (%)										
Harmonic number is varied from 1 to 5 for 660 RPM speed		k_m	e_m	c_m	$e_{fxi}(t)$	$e_{fyi}(t)$	ϕ_{exi}	ϕ_{eyi}	e_p	e_g	ϕ_p	ϕ_g
Noise	Harmonic											
5	1	–99	10	0	–4.1	–16	103	–52	1.1	0.7	–0.6	0.2
5	2	–99	10	0	–5.5	–5.6	7.6	–3.6	1.1	0.7	–0.6	0.2
5	3	–99	10	0	–9	–9	28	–13	1.1	0.7	–0.6	0.2
5	4	–99	10	0	–7	–7	47	–23	1.1	0.7	–0.6	0.2
5	5	–99	10	0	–2	–2	64	–31	1.1	0.7	–0.6	0.2
Two speeds data at 660 RPM and 1260 RPM are fed to IA												
5	1	–99	10	0	–10	–15	40	–18	1.1	0.7	–0.6	0.2

Table III shows the deviation in parameter estimates for higher harmonics from 1 to 5. These deviations are helpful in correcting the parameters of the actual gear drive for practical purposes. Also, the deviations in estimates are checked by feeding data from two speeds, which are 600 rpm apart to the IA to improve the least-squares fit estimates. The last part of Table III shows that with two speed data, the deviation in the phase of TE has reduced from 103 % to 40 %, but the same has increased the deviation in the corresponding fluctuating TE from –4.1 to –10%.

VII. GEARED-ROTOR EXPERIMENTAL PARAMETER RIG

An experimental geared-rotor system was designed and fabricated for model validation through measured vibration responses. It consists of two shafts supported on bearings, and they were connected by a gear pair as shown in Fig. 7. The test rig can accommodate different gear sets having shaft center distance (CD) varying from 45 mm to 100 mm. Threaded holes with 10 mm pitch are provided in the mounting plate to insert the shaft with bearing heads. Gear hub has 11 mm bore and 20 mm width (10 mm width is reserved for face of gear) are designed and fabricated to resist up to 50 Nm torque during the power transmission. The experimental rig consists of two parallel shafts, the drive shaft couples the motor shaft and the driven shaft, which are loaded with a torque brake. The pinion and the gear are mounted at the mid-span of these parallel shafts, which are coupled due to gear tooth meshing. The gear tooth is loaded in torsion to avoid separation of gears during the experiment by a magnetic torquer with 0.11 Nm capacity. This causes vibration at the gear mesh due to TE introduced on gear teeth, which transfers to the bearing blocks through the shafts.

The horizontal and vertical shaft displacements at gears are captured using proximity probes, which are mounted on the base plate. The eddy current-type proximity transducers have the sensitivity of 7870 mv/mm. The displacement probe placement, motor, and magnetic torquer of the experimental setup are depicted in Fig. 7. The reference

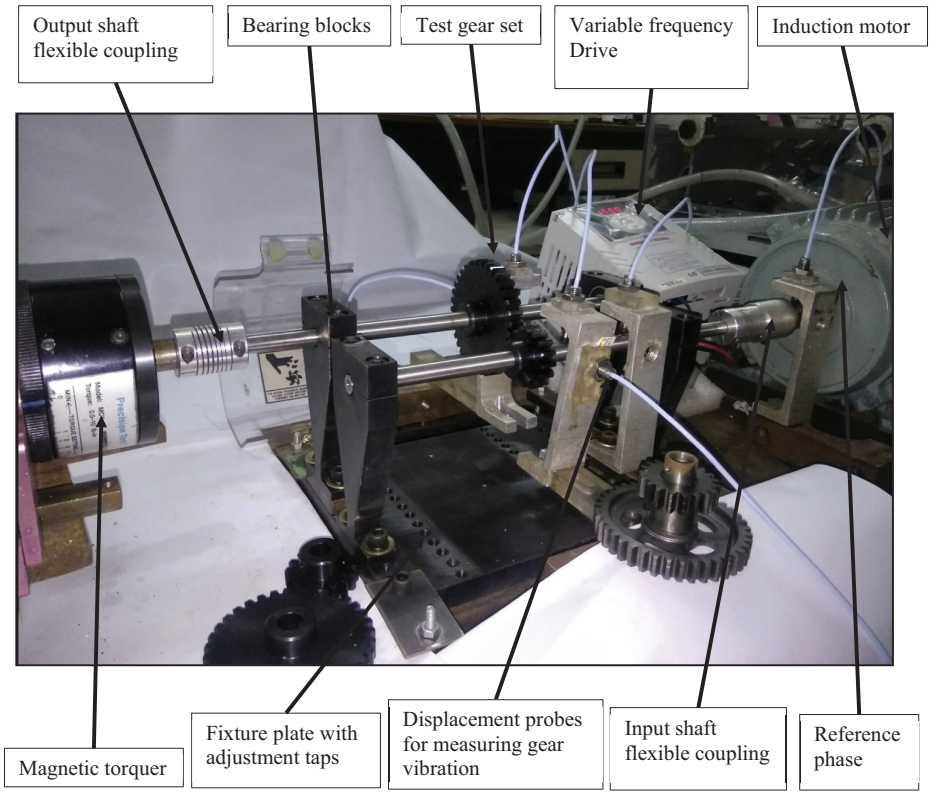

Fig. 7. Experimental rig and probe positioning at the Acoustics and Vibration lab of IIT Guwahati

signal is measured on the input shaft, close to coupling using another proximity probe. This reference signal is used for the output shaft by expanding the timescale using a gear ratio of 2.18.

The power was given to the motor through a variable frequency drive (VFD), as shown in Fig. 7, to adjust the input shaft speed. The magnetic torquer was set close to a maximum capacity of 0.1 Nm of resisting torque with the adjustment key provided with it. The experimental probes were connected to an oscilloscope to adjust the sensor with a screw to maintain a specified gap between the probe and the shaft for getting the right measurement. Each probe was connected to an eight-channel data acquisition system to digitize the signal for further processing.

The gear set has a gear ratio of 2.18 with the driven shaft mounted with a bigger gear. When viewed from the hub of gears, the torque transfer happens through the left flank. The smaller gear is fabricated with 5 μm average profile crown and 0.2 μm average lead crown. The bigger gear wheel is manufactured with 2.2 μm average profile crown and 4.5 μm average lead crown. The schematic of the crowning geometry is shown in Fig. 8.

A VFD-M power source was used as a regulator to control the speed of the motor as per the requirement of the shaft spin speed. The motor was set to run at 970 rpm (16.15 Hz) for taking measurements. The geared-rotor experimental rig was set to rotate few minutes to attain steady state condition before taking the measurement. The dSPACE DAQ system was utilized to store the measurement signal at a sampling frequency of 5,000 samples per second. A reference signal was utilized for acquiring displacement signals of the shaft for complete multiple shaft rotational cycles, that is, for $\omega t = 2\pi n$, where n is the number of complete cycles during postprocessing of acquired

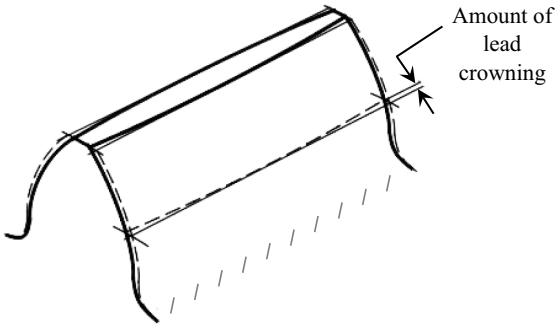

Fig. 8. Crowned spur gear tooth.

signals. Using complete cycles of signals avoids leakage error [46] and gives consistent estimates while using the IA. The horizontal and vertical measurements taken on timescale on both input and output shafts at the pinion and the gear are combined for each shaft to plot their orbits as shown in Fig. 9.

VIII. FULL-SPECTRUM RESPONSE ANALYSES FROM THE EXPERIMENTAL RIG

Gear mesh frequency of 258.4 Hz is calculated from the number of teeth in the pinion (16) multiplied by its rotational frequency (16.15 Hz). When the plots of orbits are analyzed, it is found that they are different for both input and output shafts. Also, many cycles manifested in the orbit plot specify the presence of several frequencies. Phase compensation of the measured signal is done by subtracting

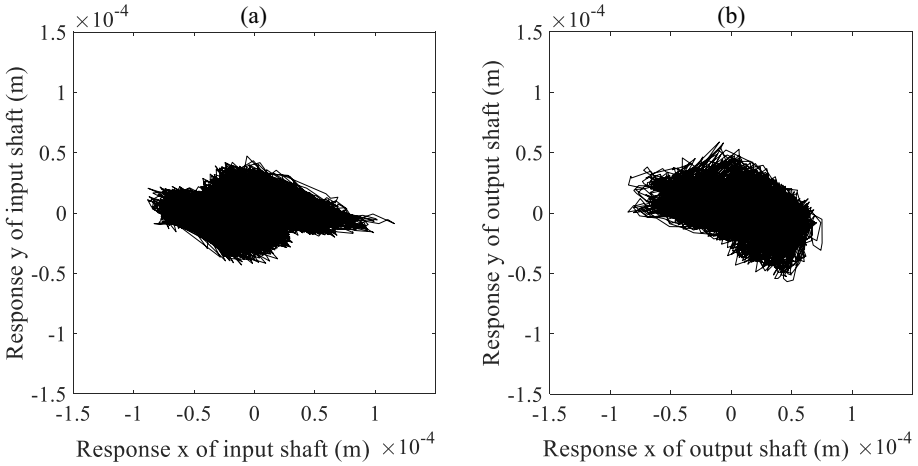

Fig. 9. Experimentally measured orbit plot of (a) drive shaft (b) driven shaft.

the phase of input and output shafts with the reference phases on the input and output shafts (output shaft phase is adjusted with the help of gear ratio) with the help of measured reference signal at the input shaft. Phase compensation helps to avoid leakage errors by synchronizing the measurements related to different harmonics present in the system.

One block of measured time domain responses is chosen for transforming them into frequency domain. The phase-compensated full-spectrum plot of experimental rig responses is shown in Fig. 10, which shows predominant peaks at five-gear mesh forward and backward whirl frequencies. These harmonics are at 258.4, 516.8, 775.2, 1033.6, and 1292 Hz. The asymmetric amplitudes of the forward and backward whirls of all five harmonics, which excite simultaneously at all harmonics, are seen in the full-spectrum response. The asymmetric full-spectrum amplitudes prove the asymmetric static TE hypothesis proposed in this research with the help of the system model and the numerical simulation in the research work.

As there is a relatively small TE of the fourth and fifth harmonics in the present gear, relatively smaller amplitude peaks are reflected in the respective frequencies in the full-spectrum response. Also, there is a relative difference in the peak amplitudes in the forward and backward whirls, which demonstrates asymmetricity in TE. Peak amplitudes at the driver and driven gear rotational frequencies are also seen at 16.15 Hz and 7.38 Hz, respectively.

IX. IDENTIFICATION OF GEAR MESH DTE PARAMETERS USING EXPERIMENTAL RIG FULL-SPECTRUM RESPONSES

After getting full-spectrum responses (both magnitude and phase) of test measured signal, the identification of the experimental rig gear mesh dynamic TE parameters is attempted in this section. Phase-compensated full-spectrum

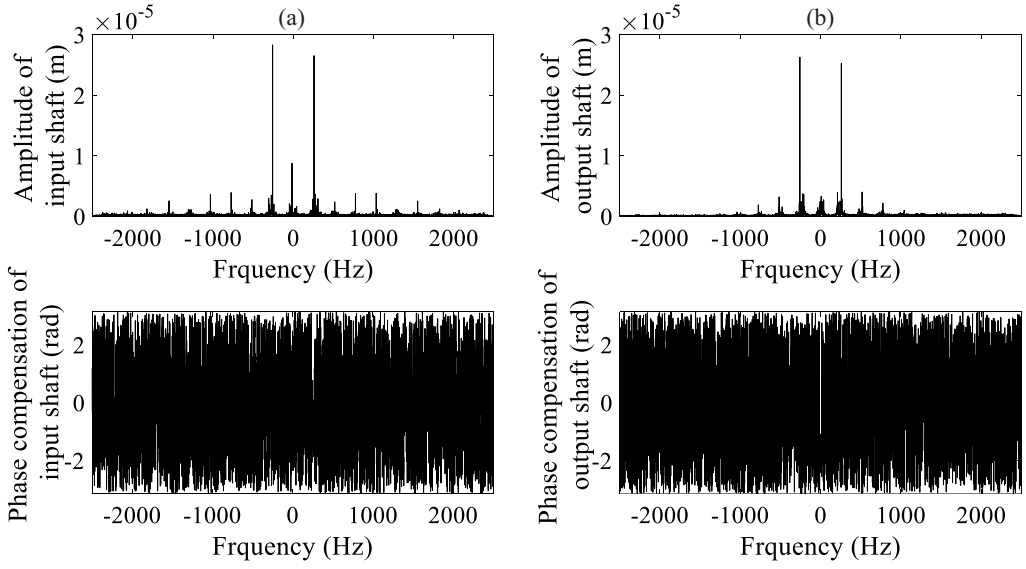

Fig. 10. (a) Full-spectrum responses of the input shaft from the experimental rig; (b) full-spectrum responses of the output shaft from the experimental rig.

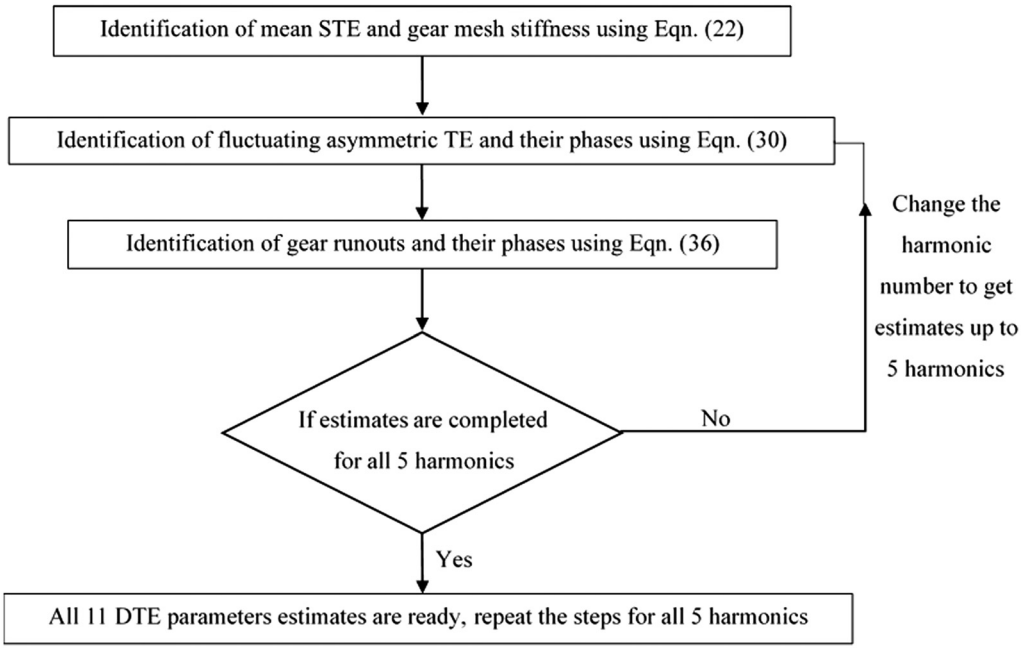

Fig. 11. Identification algorithm for the estimation of geared-rotor parameters.

responses (real and imaginary components of full-spectrum amplitudes) from the experimental rig of all the five harmonics of gear mesh frequencies along with responses at the gear and pinion shaft rotational frequency, as shown in Fig. 10, are used in the IA.

The numerically tested IA is discussed in Section IV, which has three steps in multiple parameter estimation procedure. The schematic of the three-step IA is shown in Fig. 11. These estimates are presented in Table IV. Table V shows percentage deviation of the identified parameter using the first harmonic by capturing measurements under the same operating conditions. It shows only minor deviation.

X. VALIDATION OF GEARED-ROTOR SYSTEM MODEL AND THE IA

This section is dedicated to the validation of the proposed geared-rotor system model discussed in Section II and for further validation of IA developed in Section IV. Using the full-spectrum responses measured through the experimental rig, the estimated dynamic TE parameters are obtained and presented in Table IV. These estimates are fed to the mathematical model for numerically generating the full-spectrum responses at both input and output shafts. These numerically generated full-spectrum responses are now compared with the measured full-spectrum responses from the experimental rig for validating both the system model and the IA for the correctness of estimates.

For this purpose, numerically generated full-spectrum responses of the input shaft generated with the dynamic TE parameters estimated through the experimental rig are compared with the measured full-spectrum responses from the experimental rig as shown in Fig. 12. The comparison shows perfect matching of the gear rotation frequency, pinion rotation frequency, and gear mesh frequencies up to five harmonics. Also, we can observe the perfect matching of amplitudes at the pinion and gear shaft frequencies and higher harmonics of the gear mesh

Table IV. Estimated experimental rig gear mesh DTE parameters

Parameter	Units	Identified value				
Gear mesh stiffness	N/m	23.6×10^{6}				
Mean transmission error	μm	0.23				
Gear mesh damping	Ns/m	2.445×10^{3}				
Pinion runout	μm	7.81				
Gear runout	μm	1.96				
Phase of pinion runout	rad	0.867				
Phase of gear runout	rad	2.69				
Variable TE harmonics		1^{st}	2^{nd}	3^{rd}	4^{th}	5^{th}
Variable TE in *x*-direction	μm	99.94	6.09	2.98	4.65	0.57
Variable TE in *y*-direction	μm	17.15	3.36	4.35	3.26	2.04
TE phase in *x*-direction	rad	0.49	0.65	0.97	2.33	1.47
TE phase in *y*-direction	rad	–0.40	–0.89	–1.78	–0.55	0.30

Table V. Deviation of identified parameters with repeated measurement

Experiment repeat	Percentage deviation of identified parameter by repeating test (%)										
Identified quantities are compared with Table 4 (Experiment1)	k_m	e_m	c_m	$e_{fxi}(t)$	$e_{fyi}(t)$	ϕ_{exi}	ϕ_{eyi}	e_p	e_g	ϕ_p	ϕ_g
Experiment 2	0.3	0.2	0	0.1	0	0.1	0.2	0.1	0.1	0.1	0.1
Experiment 3	0.2	0.1	0	0	0	0	0	0.07	0.07	0.01	0.1
Experiment 4	0.04	0.02	0	0	0.1	0.01	0.1	0.08	0.08	0	0
Experiment 5	0.2	0.04	0	0.1	0	0	0	0.11	0.1	0.02	0

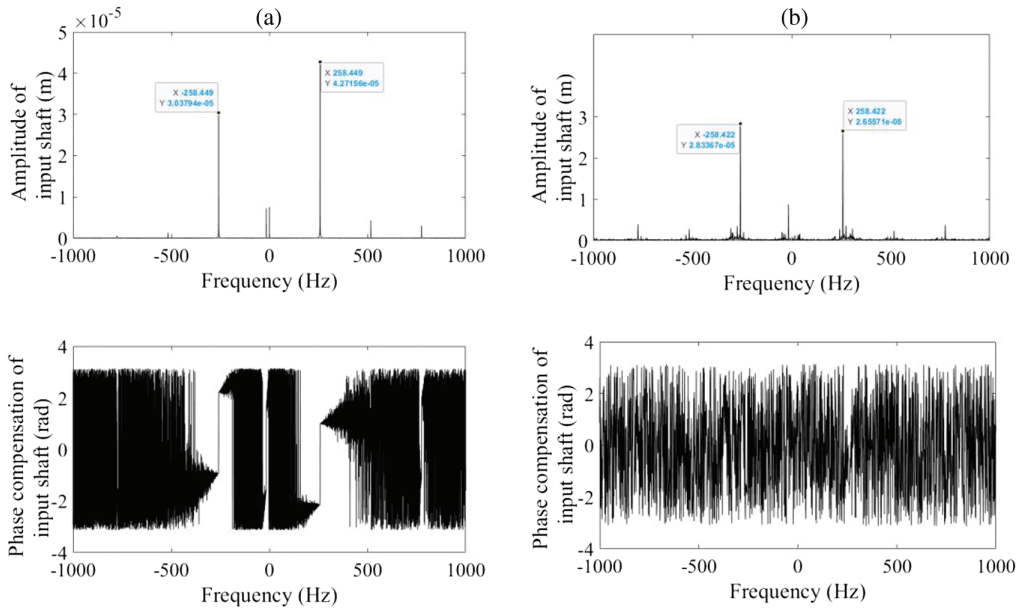

Fig. 12. (a) Numerically generated full-spectrum responses of the input shaft by feeding estimated dynamic TE parameters of the experimental rig; (b) full-spectrum responses of the input shaft from the experimental rig.

frequencies of the input shaft in Fig. 12. Here, we can also observe the asymmetry in amplitude in both forward and backward whirls at the same harmonic due to the asymmetric TE, which is present in the system model, and same is manifested in measured response from the experimental rig.

XI. CONCLUSIONS

A novel asymmetric TE-based geared-rotor system model has been developed. The equations of motion of the system model have been obtained using the Lagrangian dynamics. The response generated using time domain numerical solution is transformed into frequency domain to obtain the full-spectrum form. It depicts variable amplitudes in the forward and backward whirl frequencies.

A novel three-step IA has been developed to quantitatively identify the ten-gear mesh parameters. The algorithm is initially tested against numerically simulated full-spectrum response. This identification summary shows a stable solution even when the Gaussian measurement noise is considered in the numerical identification. Also, it is observed that the estimates improve on considering responses for more speeds.

The geared-rotor experimental rig is designed and fabricated to authenticate the system model and IA. The full-spectrum responses are generated using experimentally measured responses using displacement probes. Using the same three-step IA, the geared-rotor experimental rig parameters are identified.

Finally, in the validation part, the full-spectrum response has been plotted using experimentally estimated parameters with a numerical model and by comparing this full-spectrum plot with that of the original experimental rig full-spectrum plot. Excellent correlation between these two full-spectrum plots is observed at the input shaft. Overall, the objective of getting reasonably good estimates of all dynamic parameters of a geared-rotor system is achieved using both numerical and experimental data. The attempt to identify gear mesh dynamic parameters by linear model of the geared-rotor system using test-measured data will surely give new direction for solving gear real-world problems.

The proposed gear parameter IA facilitates researchers for identifying all the critical gear parameters using lateral vibration measurements using simple displacement probes (by simple displacement probes, it is practically easy to access gear transmission shafts with displacement probes) rather than mounting high-quality encoders to measure the TE of gear mesh by phase demodulation of the pulse signals of encoders as followed in transitional approach. The identified parameters using the proposed IA are very much helpful for researchers in a wide range of industrial

applications in automotive and aerospace applications in fault prediction, design optimization, and preventive maintenance to avoid catastrophic failures.

CONFLICT OF INTEREST STATEMENT

The authors declare no conflicts of interest.

REFERENCES

[1] R. Tiwari, "*Rotor Systems: Analysis and Identification,*" Boca Raton: CRC Press, 2017.

[2] X. Yu, Z. Li, O. He, Y. Yang, M. Du, and Z. Peng, "Gearbox fault diagnosis based on bearing dynamic force identification," *J Sound Vib,* vol. 511, p. 1, 2021.

[3] G. Majumder and R. Tiwari, "Experimental study on vibration control of spur geared rotor system with active magnetic bearings," *J Sound Vib,* vol. 532, p. 117005, 2022.

[4] N. Sarmah and R. Tiwari, "Numerical and experimental study on quantitative assessment of multiple fault parameters in a warped internally damped rotor with a transverse fatigue crack integrated with an active magnetic bearing," *Mech Syst Signal Process,* vol. 174, p. 109112, 2022.

[5] S. Ning, Y. Ren, and Y. Wu, "Intelligent fault diagnosis of rolling bearings based on the visibility algorithm and graph neural networks," *J Braz Soc Mech Sci. Eng,* vol. 45, p. 72, 2023.

[6] O. Das and D. Bagci Das, "Smart machine fault diagnostics based on fault specified discrete wavelet transform," *J Braz Soc Mech Sci. Eng,* vol. 45, p. 55, 2023.

[7] A. Choudhary, T. Mian, and S. Fatima, "Convolutional neural network based bearing fault diagnosis of rotating machine using thermal images," *Measurement,* vol. 176, p. 109196, 2021.

[8] W. Li, X. Zhong, H. Shao, B. Cai, and X. Yang, "Multi-mode data augmentation and fault diagnosis of rotating machinery using modified ACGAN designed with new framework," *Adv Eng Inform,* vol. 52, p. 101552, 2022.

[9] S. Ning, Y. Ren, and Y. Wu, "Intelligent fault diagnosis of rolling bearings based on the visibility algorithm and graph neural networks," *J Braz Soc Mech Sci. Eng,* vol. 45, p. 72, 2023.

[10] H. Walker, "Gear tooth deflections and profile modifications," *Engineer,* vol. 170, pp. 102–31, 1940.

[11] S. L. Harris, "Dynamic loads on the teeth of spur gears," *Proceedings Inst. Mech. Eng.,* vol. 172, no. 2, pp. 87–100, 1958.

[12] R. G. Munro, "A review of the theory and measurement of gear transmission error," *Proceedings First IMechE Conf. Gearbox Noise Vib.,* vol. 404, no. 032, pp. 3–10, 1990.

[13] H. N. Özgüven and D. R. Houser, "Mathematical models used in gear dynamics- a review," *J. Sound Vib.,* vol. 121, no. 3, pp. 383–411, 1988.

[14] D. Houser, "Gear noise state of the art. CETIM Internoise 88," *Avignon,* vol. 2, pp. 601–606, 1988.

[15] A. Kahraman, H. N. Özgüven, D. R. Houser, and J. Zakrajsek, "Dynamic analysis of geared-rotors by finite elements," *ASME J. Mech. Des.,* vol. 114, pp. 507–514, 1992.

[16] S. B. Wadkar and S. R. Kajale, "Mode shapes, natural frequency, and reliability of geared shaft with varying mesh stiffness," *J. Inst. Eng.,* vol. 92, pp. 32–37, 2011.

[17] O. D. Mohammed, M. Rantatalo, and J. Aidanpaa, "Improving mesh stiffness calculation of cracked gears for the purpose of vibration-based fault analysis," *Eng. Fail. Anal.,* vol. 34, pp. 235–251, 2013.

[18] C. F. Li, S. H. Zhou, J. Liu, and B. C. Wen, "Coupled lateral-torsional-axial vibrations of a helical gear-rotor-bearing system," *Acta Mech. Sin.,* vol. 30, no. 5, pp. 746–761, 2014.

[19] S. Zhou, Z. Ren, G. Song, and B. Wen, "Dynamic characteristics analysis of the coupled lateral-torsional vibration with spur gear system," *Int. J. Rotating Machinery, vol.* 2015, p. 371408, 2015.

[20] Y. Temis, D. Kalinin, and E. Kozharinov, "Simulation of gear systems with dynamic analysis," *The 14th IFToMM World Congress,* Taipei, Taiwan: Intl Federation for the Promotion of Mechanism and Machine Science (IFToMM), 2015.

[21] A. Mohamed, S. Sassi, and M. R. Paurobally, "Model-based analysis of gears' dynamic behavior in the presence of multiple cracks," J. Shock Vib., vol. 2018, pp. 1–20, 2018.

[22] B. R. Rao and V. Ganti, "Gear whine noise path analysis and mitigation strategies for automotive transmissions," *FISITA World Automotive Congress*. Bishops Stortford: FISITA (UK) Ltd, 2018.

[23] D. Southwick, "Using full-spectrum plots," *Orbit,* vol. 14, no. 4, pp. 12–16, 1993.

[24] L. Qu, A. X. Xie, and X. Li, "Study, and performance evaluation of some nonlinear diagnostic methods for large rotating machinery," *Mech. Mach. Theory,* vol. 28, no. 5, pp. 699–713, 1993.

[25] D. Southwick, "Using full-spectrum plots: Part 2," *Orbit,* vol. 15, no. 2, pp. 10–11, 1994.

[26] P. Goldman and A. Muszynska, "Application of full-spectrum to rotating machinery diagnostics," *Orbit First Quarter,* vol. 1, pp. 17–21, 1999.

[27] N. Bachschmid, P. Pennacchi, and A. Vania, "Diagnostic significance of orbit shape analysis and its application to improve machine fault detection," *J. Braz Society Mech. Sci. Engineering,* vol. 2, pp. 200–208, 2004.

[28] J. Tuma and J. Bilos, "Fluid instability of rotor systems with journal bearings," *Engineering Mech.,* vol. 14, pp. 69–80, 2007.

[29] T. H. Patel and A. K. Darpe, "Application of full-spectrum analysis for rotor fault diagnosis," Proceedings IUTAM Symp. Emerging Trends Rotor Dyn., vol. 1011, pp. 535–545, 2009.

[30] C. Shravankumar and R. Tiwari, "Model-based crack identification using full-spectrum," *ASME Gas Turbine India Conference*. New York City: ASME, 2013.

[31] L. Hong and J. S. Dhupia, "A time domain approach to diagnose gearbox fault based on measured vibration signals," *J. Sound Vib.,* vol. 333, pp. 2164–2180, 2014.

[32] N. Sawalhi and R. B. Randall, "Gear parameter identification in a wind turbine gearbox using vibration signals," Mech. Syst., Sign. Proc., vol. 42, pp. 368–376, 2014.

[33] Z. Feng, X. Chen, and M. Liang, "Joint envelope and frequency order spectrum analysis based on iterative generalized demodulation for planetary gearbox fault diagnosis under nonstationary conditions," *Mech. Syst. Sig. Process.,* vol. 76–77, pp. 242–264, 2016.

[34] O. Dogan and F. Karpat, "Crack detection for spur gears with asymmetric teeth based on the dynamic transmission error," *Mech. Mach. Theory,* vol. 133, pp. 417–431, 2019.

[35] M. Benatar, M. Handschuh, A. Kahraman, D. Talbot, "Static and dynamic transmission error measurements of helical gear pairs with various tooth modifications," *J Mech N Y,* vol. 141, p. 103301, 2019.

[36] A. Celikay, A. Donmez, and A. Kahraman, "An experimental and theoretical study of subharmonic resonances of a spur gear pair," *J. Sound Vib.,* vol. 515, p. 116421, 2021.

[37] J. Flek, M. Dub, J. Kolár, F. Lopot, and K. Petr, "Determination of Mesh Stiffness of Gear-Analytical Approach vs. FEM Analysis," *Appl. Sci.,* vol. 11, p. 4960, 2021.

[38] Z. Y. Chin, P. Borghesani, Y. Mao, W. A. Smith, and R. B. Randall, "Use of transmission error for a quantitative estimation of root-crack severity in gears," *Mech. Syst. Sig. Process.,* vol. 171, p. 108957, 2022.

[39] S. Xue, I. Howard, C. Wang, P. Lian, Y. Wang, and G. Liu, "Dynamic modelling of the gear system under non-stationary conditions using the iterative convergence of the tooth mesh stiffness," *Eng. Fail. Anal.,* vol. 131, p. 105908, 2022.

[40] J. C. Poletto, C. M. C. G. Fernandes, L. Y. Barros, P. D. Neis, K. Pondicherry, D. Fauconnier, J. H. O. Seabra, P. D. Baets, and N. F. Ferreira, "Identification of gear wear damage using topography analysis," *Wear,* vol. 522, p. 204837, 2023.

[41] P. Dai, X. Liang, J. Wang, F. Wang, and T. T. Sun, "Mathematical model for mesh analysis of gear pair in gear-shaft-bearing systems with localized failure on raceway," *J. Sound Vib.,* vol. 584, p. 118458, 2024.

[42] A. Talakesh, S. H. Jazi, A. Ariaei, and A. Poursina, "A new experimental method for calculating mesh stiffness in healthy and cracked straight bevel gear system," *Measurement,* vol. 224, p. 113804, 2024.

[43] X. Dong, Y. Huangfu, X. Yu, K. Chen, Z. Li, and Z. Peng, "Identification of the error excitation in gear systems: a mediator algorithm between simulation and experiment," *J. Sound Vib.,* vol. 568, p. 118060, 2024.

[44] J. Koutsoupakis, P. Seventekidis, and D. Giagopoulos, "Machine learning based condition monitoring for gear transmission systems using data generated by optimal multibody dynamics models," *Mech. Syst. Sig. Process.,* vol. 190, p. 110130, 2023.

[45] B. R. Rao and R. Tiwari, "Detection of asymmetric transmission error in geared-rotor system through transverse vibration analysis using full-spectrum," *Propul. Power Res.,* vol. 9, no. 3, pp. 255–280, 2020.

[46] S. Singh and R. Tiwari, "Model-based fatigue crack identification in rotors integrated with active magnetic bearings," *J. Vib. Control,* vol. 23, no. 6, pp. 980–1000, 2015.

Appendix A.Time domain to frequency domain transformation using Euler's complex identity

From Euler's complex identity, we can convert the exponential terms into the sine and cosine terms as,

$$e^{\mathrm{j}(\omega_p t+\phi_p)} = \{\cos(\omega_p t+\phi_p) + \mathrm{j}\sin(\omega_p t+\phi_p)\}; \quad e^{-\mathrm{j}(\omega_p t+\phi_p)} = \{\cos(\omega_p t+\phi_p) - \mathrm{j}\sin(\omega_p t+\phi_p)\} \tag{A-1}$$

$$e^{\mathrm{j}(\omega_g t+\phi_g)} = \{\cos(\omega_g t+\phi_g) + \mathrm{j}\sin(\omega_g t+\phi_g)\}; \quad e^{-\mathrm{j}(\omega_g t+\phi_g)} = \{\cos(\omega_g t+\phi_g) - \mathrm{j}\sin(\omega_g t+\phi_g)\} \tag{A-2}$$

$$e^{\mathrm{j}(\omega_e t+\phi_e)} = \{\cos(\omega_e t+\phi_e) + \mathrm{j}\sin(\omega_e t+\phi_e)\}; \quad e^{-\mathrm{j}(\omega_e t+\phi_e)} = \{\cos(\omega_e t+\phi_e) - \mathrm{j}\sin(\omega_e t+\phi_e)\} \tag{A-3}$$

which gives

$$\sin(\omega_p t+\phi_p) = (e^{\mathrm{j}(\omega_p t+\phi_p)} - e^{-\mathrm{j}(\omega_p t+\phi_p)})/2\mathrm{j}; \quad \cos(\omega_p t+\phi_p) = (e^{\mathrm{j}(\omega_p t+\phi_p)} + e^{-\mathrm{j}(\omega_p t+\phi_p)})/2 \tag{A-4}$$

$$\sin(\omega_g t+\phi_g) = (e^{\mathrm{j}(\omega_g t+\phi_g)} - e^{-\mathrm{j}(\omega_g t+\phi_g)})/2\mathrm{j}; \quad \cos(\omega_g t+\phi_g) = (e^{\mathrm{j}(\omega_g t+\phi_g)} + e^{-\mathrm{j}(\omega_g t+\phi_g)})/2 \tag{A-5}$$

$$\sin(\omega_e t+\phi_e) = (e^{\mathrm{j}(\omega_e t+\phi_e)} - e^{-\mathrm{j}(\omega_e t+\phi_e)})/2\mathrm{j}; \quad \cos(\omega_e t+\phi_e) = (e^{\mathrm{j}(\omega_e t+\phi_e)} + e^{-\mathrm{j}(\omega_e t+\phi_e)})/2 \tag{A-6}$$

On substituting above equations (A-4) to (A-6) in the force vector, equation (14), as,

$$\mathbf{f}(t) = \left\{ \begin{array}{c}
k_m e_m + 0.5 m_1 e_p \omega_p^2 (e^{\mathrm{j}(\omega_p t+\phi_p)} + e^{-\mathrm{j}(\omega_p t+\phi_p)}) \\
+(0.5c_m/\mathrm{j}) \left(\begin{array}{c} e_p\omega_p(e^{\mathrm{j}(\omega_p t+\phi_p)} - e^{-\mathrm{j}(\omega_p t+\phi_p)}) - e_g\omega_g(e^{\mathrm{j}(\omega_g t+\phi_g)} - e^{-\mathrm{j}(\omega_g t+\phi_g)}) \\ +\mathrm{j}\sum_{i=1}^{n} e_{f_{xi}} i\omega_e (e^{\mathrm{j}(i\omega_e t+\phi_{e_{xi}})} + e^{-\mathrm{j}(i\omega_e t+\phi_{e_{xi}})}) \end{array} \right) \\
+(0.5k_m/\mathrm{j}) \left(\begin{array}{c} -\mathrm{j}e_p(e^{\mathrm{j}(\omega_p t+\phi_p)} + e^{-\mathrm{j}(\omega_p t+\phi_p)}) + \mathrm{j}e_g(e^{\mathrm{j}(\omega_g t+\phi_g)} + e^{-\mathrm{j}(\omega_g t+\phi_g)}) \\ +(\sum_{i=1}^{n} e_{f_{xi}} (e^{\mathrm{j}(i\omega_e t+\phi_{e_{xi}})} - e^{-\mathrm{j}(i\omega_e t+\phi_{e_{xi}})})) \end{array} \right) \\
+(0.5c_{s1}/\mathrm{j})(e_p\omega_p(e^{\mathrm{j}(\omega_p t+\phi_p)} - e^{-\mathrm{j}(\omega_p t+\phi_p)})) - (0.5k_{s1})(e_p(e^{\mathrm{j}(\omega_p t+\phi_p)} + e^{-\mathrm{j}(\omega_p t+\phi_p)})) \\
-m_1 g + k_m e_m - 0.5 m_1 e_p \omega_p^2 (e^{\mathrm{j}(\omega_p t+\phi_p)} - e^{-\mathrm{j}(\omega_p t+\phi_p)})/\mathrm{j} \\
+(0.5c_m/\mathrm{j}) \left(\begin{array}{c} \mathrm{j}e_p\omega_p(e^{\mathrm{j}(\omega_p t+\phi_p)} + e^{-\mathrm{j}(\omega_p t+\phi_p)}) + \mathrm{j}e_g\omega_g(e^{\mathrm{j}(\omega_g t+\phi_g)} + e^{-\mathrm{j}(\omega_g t+\phi_g)}) \\ +\mathrm{j}\sum_{i=1}^{n} e_{f_{yi}} i\omega_e (e^{\mathrm{j}(i\omega_e t+\phi_{e_{yi}})} + e^{-\mathrm{j}(i\omega_e t+\phi_{e_{yi}})}) \end{array} \right) \\
+(0.5k_m/\mathrm{j}) \left(\begin{array}{c} e_p(e^{\mathrm{j}(\omega_p t+\phi_p)} - e^{-\mathrm{j}(\omega_p t+\phi_p)}) + e_g(e^{\mathrm{j}(\omega_g t+\phi_g)} - e^{-\mathrm{j}(\omega_g t+\phi_g)}) \\ +\sum_{i=1}^{n} e_{f_{yi}} (e^{\mathrm{j}(i\omega_e t+\phi_{e_{yi}})} - e^{-\mathrm{j}(i\omega_e t+\phi_{e_{yi}})}) \end{array} \right) \\
+(0.5c_{s1})(e_p\omega_p(e^{\mathrm{j}(\omega_p t+\phi_p)} + e^{-\mathrm{j}(\omega_p t+\phi_p)})) + (0.5k_{s1}/\mathrm{j})(e_p(e^{\mathrm{j}(\omega_p t+\phi_p)} - e^{-\mathrm{j}(\omega_p t+\phi_p)})) \\
-k_m e_m + 0.5 m_2 e_g \omega_g^2 (e^{\mathrm{j}(\omega_g t+\phi_g)} + e^{-\mathrm{j}(\omega_g t+\phi_g)}) \\
-(0.5c_m/\mathrm{j}) \left(\begin{array}{c} e_p\omega_p(e^{\mathrm{j}(\omega_p t+\phi_p)} - e^{-\mathrm{j}(\omega_p t+\phi_p)}) - e_g\omega_g(e^{\mathrm{j}(\omega_g t+\phi_g)} - e^{-\mathrm{j}(\omega_g t+\phi_g)}) \\ +\mathrm{j}\sum_{i=1}^{n} e_{f_{xi}} i\omega_e (e^{\mathrm{j}(i\omega_e t+\phi_{e_{xi}})} + e^{-\mathrm{j}(i\omega_e t+\phi_{e_{xi}})}) \end{array} \right) \\
-(0.5k_m/\mathrm{j}) \left(\begin{array}{c} -e_p\mathrm{j}(e^{\mathrm{j}(\omega_p t+\phi_p)} + e^{-\mathrm{j}(\omega_p t+\phi_p)}) + e_g\mathrm{j}(e^{\mathrm{j}(\omega_g t+\phi_g)} + e^{-\mathrm{j}(\omega_g t+\phi_g)}) \\ +\sum_{i=1}^{n} e_{f_{xi}} (e^{\mathrm{j}(i\omega_e t+\phi_{e_{xi}})} - e^{-\mathrm{j}(i\omega_e t+\phi_{e_{xi}})}) \end{array} \right) \\
+(0.5c_{s2}/\mathrm{j})(e_g\omega_g(e^{\mathrm{j}(\omega_g t+\phi_g)} - e^{-\mathrm{j}(\omega_g t+\phi_g)})) - (0.5k_{s2})(e_g(e^{\mathrm{j}(\omega_g t+\phi_g)} + e^{-\mathrm{j}(\omega_g t+\phi_g)})) \\
-m_2 g - k_m e_m + 0.5 m_2 e_g \omega_g^2 (e^{\mathrm{j}(\omega_g t+\phi_g)} - e^{-\mathrm{j}(\omega_g t+\phi_g)})/\mathrm{j} \\
-(0.5c_m/\mathrm{j}) \left(\begin{array}{c} \mathrm{j}e_p\omega_p(e^{\mathrm{j}(\omega_p t+\phi_p)} + e^{-\mathrm{j}(\omega_p t+\phi_p)}) + \mathrm{j}e_g\omega_g(e^{\mathrm{j}(\omega_g t+\phi_g)} + e^{-\mathrm{j}(\omega_g t+\phi_g)}) \\ +\mathrm{j}\sum_{i=1}^{n} e_{f_{yi}} i\omega_e (e^{\mathrm{j}(i\omega_e t+\phi_{e_{yi}})} + e^{-\mathrm{j}(i\omega_e t+\phi_{e_{yi}})}) \end{array} \right) \\
-(0.5k_m/\mathrm{j}) \left(\begin{array}{c} e_p(e^{\mathrm{j}(\omega_p t+\phi_p)} - e^{-\mathrm{j}(\omega_p t+\phi_p)}) + e_g(e^{\mathrm{j}(\omega_g t+\phi_g)} - e^{-\mathrm{j}(\omega_g t+\phi_g)}) \\ +\sum_{i=1}^{n} e_{f_{yi}} (e^{\mathrm{j}(i\omega_e t+\phi_{e_{yi}})} - e^{-\mathrm{j}(i\omega_e t+\phi_{e_{yi}})}) \end{array} \right) \\
-(0.5c_{s2})(e_g\omega_g(e^{\mathrm{j}(\omega_g t+\phi_g)} + e^{-\mathrm{j}(\omega_g t+\phi_g)})) - (0.5k_{s2}/\mathrm{j})(e_g(e^{\mathrm{j}(\omega_g t+\phi_g)} - e^{-\mathrm{j}(\omega_g t+\phi_g)}))
\end{array} \right\} \tag{A-7}$$

The force given in Eqn. (14) is acting at the gear mesh pitch point, which is resolved in the x and y components. Forces are now split into various components as follows,

$$\mathbf{f}(t) = \begin{Bmatrix} k_m e_m \\ -m_1 g + k_m e_m \\ -k_m e_m \\ -m_2 g - k_m e_m \end{Bmatrix} + \frac{1}{2\mathrm{j}} \begin{Bmatrix} \mathrm{j} m_1 e_p \omega_p^2 (e^{\mathrm{j}(\omega_p t+\phi_p)} + e^{-\mathrm{j}(\omega_p t+\phi_p)}) \\ -m_1 e_p \omega_p^2 (e^{\mathrm{j}(\omega_p t+\phi_p)} - e^{-\mathrm{j}(\omega_p t+\phi_p)}) \\ \mathrm{j} m_2 e_g \omega_g^2 (e^{\mathrm{j}(\omega_g t+\phi_g)} + e^{-\mathrm{j}(\omega_g t+\phi_g)}) \\ m_2 e_g \omega_g^2 (e^{\mathrm{j}(\omega_g t+\phi_g)} - e^{-\mathrm{j}(\omega_g t+\phi_g)}) \end{Bmatrix}$$

$$+ \begin{Bmatrix} \frac{c_{s1}}{2\mathrm{j}} e_p \omega_p (e^{\mathrm{j}(\omega_p t+\phi_p)} - e^{-\mathrm{j}(\omega_p t+\phi_p)}) \\ \frac{c_{s1}}{2\mathrm{j}} \mathrm{j} e_p \omega_p (e^{\mathrm{j}(\omega_p t+\phi_p)} + e^{-\mathrm{j}(\omega_p t+\phi_p)}) \\ \frac{c_{s2}}{2\mathrm{j}} e_g \omega_g (e^{\mathrm{j}(\omega_g t+\phi_g)} - e^{-\mathrm{j}(\omega_g t+\phi_g)}) \\ -\frac{c_{s2}}{2\mathrm{j}} \mathrm{j} e_g \omega_g (e^{\mathrm{j}(\omega_g t+\phi_g)} + e^{-\mathrm{j}(\omega_g t+\phi_g)}) \end{Bmatrix}$$

$$+ \begin{Bmatrix} -\frac{k_{s1}}{2\mathrm{j}} \mathrm{j} e_p (e^{\mathrm{j}(\omega_p t+\phi_p)} + e^{-\mathrm{j}(\omega_p t+\phi_p)}) \\ \frac{k_{s1}}{2\mathrm{j}} e_p (e^{\mathrm{j}(\omega_p t+\phi_p)} - e^{-\mathrm{j}(\omega_p t+\phi_p)}) \\ -\frac{k_{s2}}{2\mathrm{j}} \mathrm{j} e_g (e^{\mathrm{j}(\omega_g t+\phi_g)} + e^{-\mathrm{j}(\omega_g t+\phi_g)}) \\ -\frac{k_{s2}}{2\mathrm{j}} e_g (e^{\mathrm{j}(\omega_g t+\phi_g)} - e^{-\mathrm{j}(\omega_g t+\phi_g)}) \end{Bmatrix} \quad \frac{c_m}{2\mathrm{j}} \begin{Bmatrix} e_p \omega_p (e^{\mathrm{j}(\omega_p t+\phi_p)} - e^{-\mathrm{j}(\omega_p t+\phi_p)}) - e_g \omega_g (e^{\mathrm{j}(\omega_g t+\phi_g)} - e^{-\mathrm{j}(\omega_g t+\phi_g)}) \\ \mathrm{j} e_p \omega_p (e^{\mathrm{j}(\omega_p t+\phi_p)} + e^{-\mathrm{j}(\omega_p t+\phi_p)}) + \mathrm{j} e_g \omega_g (e^{\mathrm{j}(\omega_g t+\phi_g)} + e^{-\mathrm{j}(\omega_g t+\phi_g)}) \\ -e_p \omega_p (e^{\mathrm{j}(\omega_p t+\phi_p)} - e^{-\mathrm{j}(\omega_p t+\phi_p)}) + e_g \omega_g (e^{\mathrm{j}(\omega_g t+\phi_g)} - e^{-\mathrm{j}(\omega_g t+\phi_g)}) \\ -\mathrm{j} e_p \omega_p (e^{\mathrm{j}(\omega_p t+\phi_p)} + e^{-\mathrm{j}(\omega_p t+\phi_p)}) - \mathrm{j} e_g \omega_g (e^{\mathrm{j}(\omega_g t+\phi_g)} + e^{-\mathrm{j}(\omega_g t+\phi_g)}) \end{Bmatrix}$$

$$+ \frac{c_m}{2} \sum_{i=1}^{n} \begin{Bmatrix} i(e_{xi} \omega_e (e^{\mathrm{j}(i\omega_e t+\phi_{e_{xi}})} + e^{-\mathrm{j}(i\omega_e t+\phi_{e_{xi}})})) \\ +\mathrm{j}(i e_{yi} \omega_e (e^{\mathrm{j}(i\omega_e t+\phi_{e_{yi}})} + e^{-\mathrm{j}(i\omega_e t+\phi_{e_{yi}})})) \\ i(-e_{xi} \omega_e (e^{\mathrm{j}(i\omega_e t+\phi_{e_{xi}})} + e^{-\mathrm{j}(i\omega_e t+\phi_{e_{xi}})})) \\ +\mathrm{j}(-i e_{yi} \omega_e (e^{\mathrm{j}(i\omega_e t+\phi_{e_{yi}})} + e^{-\mathrm{j}(i\omega_e t+\phi_{e_{yi}})})) \end{Bmatrix}$$

$$\frac{k_m}{2\mathrm{j}} \begin{Bmatrix} -\mathrm{j} e_p (e^{\mathrm{j}(\omega_p t+\phi_p)} + e^{-\mathrm{j}(\omega_p t+\phi_p)}) + \mathrm{j} e_g (e^{\mathrm{j}(\omega_g t+\phi_g)} + e^{-\mathrm{j}(\omega_g t+\phi_g)}) \\ e_p (e^{\mathrm{j}(\omega_p t+\phi_p)} - e^{-\mathrm{j}(\omega_p t+\phi_p)}) + e_g (e^{\mathrm{j}(\omega_g t+\phi_g)} - e^{-\mathrm{j}(\omega_g t+\phi_g)}) \\ \mathrm{j} e_p (e^{\mathrm{j}(\omega_p t+\phi_p)} + e^{-\mathrm{j}(\omega_p t+\phi_p)}) - \mathrm{j} e_g \omega_g (e^{\mathrm{j}(\omega_g t+\phi_g)} + e^{-\mathrm{j}(\omega_g t+\phi_g)}) \\ -e_p (e^{\mathrm{j}(\omega_p t+\phi_p)} - e^{-\mathrm{j}(\omega_p t+\phi_p)}) - e_g (e^{\mathrm{j}(\omega_g t+\phi_g)} - e^{-\mathrm{j}(\omega_g t+\phi_g)}) \end{Bmatrix}$$

$$+ \frac{k_m}{2\mathrm{j}} \sum_{i=1}^{n} \begin{bmatrix} e_{xi} (e^{\mathrm{j}(i\omega_e t+\phi_{e_{xi}})} - e^{-\mathrm{j}(i\omega_e t+\phi_{e_{xi}})}) \\ e_{yi} (e^{\mathrm{j}(i\omega_e t+\phi_{e_{yi}})} - e^{-\mathrm{j}(i\omega_e t+\phi_{e_{yi}})}) \\ -e_{xi} (e^{\mathrm{j}(i\omega_e t+\phi_{e_{xi}})} - e^{-\mathrm{j}(i\omega_e t+\phi_{e_{xi}})}) \\ -e_{yi} (e^{\mathrm{j}(i\omega_e t+\phi_{e_{yi}})} - e^{-\mathrm{j}(i\omega_e t+\phi_{e_{yi}})}) \end{bmatrix} \tag{A-8}$$

Now, defining complex displacements as,

$$r_1 = x_1 + \mathrm{j} y_1 \text{ and } \quad r_2 = x_2 + \mathrm{j} y_2 \tag{A-9}$$

The equations of motion Eqn. (11) can be written, in terms of the complex displacements as given in equation (A-9) as,

$$m_1 \ddot{r}_1 + (c_{s1} + c_m)\dot{r}_1 - c_m \dot{r}_2 + (k_{s1} + k_m) r_1 - k_m r_2 = f_{r1}(t) \tag{A-10}$$

$$m_2 \ddot{r}_2 + (c_{s2} - c_m)\dot{r}_2 - c_m \dot{r}_1 + (k_{s2} + k_m) r_2 - k_m r_1 = f_{r2}(t) \tag{A-11}$$

with

$$f_{r1}(t) = f_{x1} + \mathrm{j} f_{y1} \qquad \text{and} \qquad f_{r2}(t) = f_{x2} + \mathrm{j} f_{y2} \tag{A-12}$$

Defining a force vector in complex form as,

$$\mathbf{f}_r(t) = \begin{Bmatrix} f_{r1}(t) \\ f_{r2}(t) \end{Bmatrix} = \begin{Bmatrix} f_{x1} + \mathrm{j} f_{y1} \\ f_{x2} + \mathrm{j} f_{y2} \end{Bmatrix} \tag{A-13}$$

Replacing for force component terms form Eqn. (A-7), to get

$$
\begin{aligned}
\mathbf{f}_r(t) = &\left\{ \begin{array}{c} (k_m e_m) + \mathrm{j}(-m_1 g + k_m e_m) \\ (-k_m e_m) + \mathrm{j}(-m_2 g - k_m e_m) \end{array} \right\} + \frac{1}{2} \left\{ \begin{array}{c} m_1 e_p \omega_p^2 (e^{\mathrm{j}(\omega_p t+\phi_p)} + e^{-\mathrm{j}(\omega_p t+\phi_p)}) \\ -m_1 e_p \omega_p^2 (e^{\mathrm{j}(\omega_p t+\phi_p)} - e^{-\mathrm{j}(\omega_p t+\phi_p)}) \\ m_2 e_g \omega_g^2 (e^{\mathrm{j}(\omega_g t+\phi_g)} + e^{-\mathrm{j}(\omega_g t+\phi_g)}) \\ + m_2 e_g \omega_g^2 (e^{\mathrm{j}(\omega_g t+\phi_g)} - e^{-\mathrm{j}(\omega_g t+\phi_g)}) \end{array} \right\} \\
&+ \left\{ \begin{array}{c} \frac{c_{s1}}{2\mathrm{j}} e_p \omega_p (e^{\mathrm{j}(\omega_p t+\phi_p)} - e^{-\mathrm{j}(\omega_p t+\phi_p)}) + \mathrm{j}\frac{c_{s1}}{2\mathrm{j}} \mathrm{j} e_p \omega_p (e^{\mathrm{j}(\omega_p t+\phi_p)} + e^{-\mathrm{j}(\omega_p t+\phi_p)}) \\ \frac{c_{s2}}{2\mathrm{j}} e_g \omega_g (e^{\mathrm{j}(\omega_g t+\phi_g)} - e^{-\mathrm{j}(\omega_g t+\phi_g)}) - \mathrm{j}\frac{c_{s2}}{2\mathrm{j}} \mathrm{j} e_g \omega_g (e^{\mathrm{j}(\omega_g t+\phi_g)} + e^{-\mathrm{j}(\omega_g t+\phi_g)}) \end{array} \right\} \\
&+ \left\{ \begin{array}{c} -\frac{k_{s1}}{2\mathrm{j}} \mathrm{j} e_p (e^{\mathrm{j}(\omega_p t+\phi_p)} + e^{-\mathrm{j}(\omega_p t+\phi_p)}) + j\frac{k_{s1}}{2\mathrm{j}} e_p (e^{\mathrm{j}(\omega_p t+\phi_p)} - e^{-\mathrm{j}(\omega_p t+\phi_p)}) \\ -\frac{k_{s2}}{2\mathrm{j}} \mathrm{j} e_g (e^{\mathrm{j}(\omega_g t+\phi_g)} + e^{-\mathrm{j}(\omega_g t+\phi_g)}) - j\frac{k_{s2}}{2\mathrm{j}} e_g (e^{\mathrm{j}(\omega_g t+\phi_g)} - e^{-\mathrm{j}(\omega_g t+\phi_g)}) \end{array} \right\} \\
&+ \frac{c_m}{2} \left\{ \begin{array}{c} -\mathrm{j} e_p \omega_p (e^{\mathrm{j}(\omega_p t+\phi_p)} - e^{-\mathrm{j}(\omega_p t+\phi_p)}) + \mathrm{j} e_g \omega_g (e^{\mathrm{j}(\omega_g t+\phi_g)} - e^{-\mathrm{j}(\omega_g t+\phi_g)}) \\ + \mathrm{j} e_p \omega_p (e^{\mathrm{j}(\omega_p t+\phi_p)} + e^{-\mathrm{j}(\omega_p t+\phi_p)}) + \mathrm{j} e_g \omega_g (e^{\mathrm{j}(\omega_g t+\phi_g)} + e^{-\mathrm{j}(\omega_g t+\phi_g)}) \\ \mathrm{j} e_p \omega_p (e^{\mathrm{j}(\omega_p t+\phi_p)} - e^{-\mathrm{j}(\omega_p t+\phi_p)}) - \mathrm{j} e_g \omega_g (e^{\mathrm{j}(\omega_g t+\phi_g)} - e^{-\mathrm{j}(\omega_g t+\phi_g)}) \\ -\mathrm{j} e_p \omega_p (e^{\mathrm{j}(\omega_p t+\phi_p)} + e^{-\mathrm{j}(\omega_p t+\phi_p)}) - \mathrm{j} e_g \omega_g (e^{\mathrm{j}(\omega_g t+\phi_g)} + e^{-\mathrm{j}(\omega_g t+\phi_g)}) \end{array} \right\} \\
&+ \frac{k_m}{2} \left\{ \begin{array}{c} -e_p (e^{\mathrm{j}(\omega_p t+\phi_p)} + e^{-\mathrm{j}(\omega_p t+\phi_p)}) + e_g (e^{\mathrm{j}(\omega_g t+\phi_g)} + e^{-\mathrm{j}(\omega_g t+\phi_g)}) \\ + e_p (e^{\mathrm{j}(\omega_p t+\phi_p)} - e^{-\mathrm{j}(\omega_p t+\phi_p)}) + e_g (e^{\mathrm{j}(\omega_g t+\phi_g)} - e^{-\mathrm{j}(\omega_g t+\phi_g)}) \\ e_p (e^{\mathrm{j}(\omega_p t+\phi_p)} + e^{-\mathrm{j}(\omega_p t+\phi_p)}) - e_g \omega_g (e^{\mathrm{j}(\omega_g t+\phi_g)} + e^{-\mathrm{j}(\omega_g t+\phi_g)}) \\ -e_p (e^{\mathrm{j}(\omega_p t+\phi_p)} - e^{-\mathrm{j}(\omega_p t+\phi_p)}) - e_g (e^{\mathrm{j}(\omega_g t+\phi_g)} - e^{-\mathrm{j}(\omega_g t+\phi_g)}) \end{array} \right\} \\
&+ \frac{c_m}{2} \sum_{i=1}^{n} \left\{ \begin{array}{c} i(e_{xi} \omega_e (e^{\mathrm{j}(i\omega_e t+\phi_{e_{xi}})} + e^{-\mathrm{j}(i\omega_e t+\phi_{e_{xi}})})) \\ + \mathrm{j}(i e_{yi} \omega_e (e^{\mathrm{j}(i\omega_e t+\phi_{e_{yi}})} + e^{-\mathrm{j}(i\omega_e t+\phi_{e_{yi}})})) \\ i(-e_{xi} \omega_e (e^{\mathrm{j}(i\omega_e t+\phi_{e_{xi}})} + e^{-\mathrm{j}(i\omega_e t+\phi_{e_{xi}})})) \\ + \mathrm{j}(-i e_{yi} \omega_e (e^{\mathrm{j}(i\omega_e t+\phi_{e_{yi}})} + e^{-\mathrm{j}(i\omega_e t+\phi_{e_{yi}})})) \end{array} \right\} \\
&+ \frac{k_m}{2} \sum_{i=1}^{n} \left\{ \begin{array}{c} -\mathrm{j}(e_{xi} (e^{\mathrm{j}(i\omega_e t+\phi_{e_{xi}})} - e^{-\mathrm{j}(i\omega_e t+\phi_{e_{xi}})}) \\ (i e_{yi} (e^{\mathrm{j}(i\omega_e t+\phi_{e_{yi}})} - e^{-\mathrm{j}(i\omega_e t+\phi_{e_{yi}})})) \\ (+ \mathrm{j} e_{xi} (e^{\mathrm{j}(i\omega_e t+\phi_{e_{xi}})} - e^{-\mathrm{j}(i\omega_e t+\phi_{e_{xi}})})) \\ (-i e_{yi} (e^{\mathrm{j}(i\omega_e t+\phi_{e_{yi}})} - e^{-\mathrm{j}(i\omega_e t+\phi_{e_{yi}})})) \end{array} \right\}
\end{aligned}
\tag{A-14}
$$

On collecting similar exponential terms, to get

$$
\begin{aligned}
\mathbf{f}_r(t) = &\left\{ \begin{array}{c} (k_m e_m) + \mathrm{j}(-m_1 g + k_m e_m) \\ (-k_m e_m) + \mathrm{j}(-m_2 g - k_m e_m) \end{array} \right\} \\
&+ \left\{ \begin{array}{c} m_1 e_p \omega_p^2 e^{-\mathrm{j}\phi_p} e^{-\mathrm{j}\omega_p t} + \mathrm{j} c_m e_p \omega_p e^{-\mathrm{j}\phi_p} e^{-\mathrm{j}\omega_p t} + \mathrm{j} c_m e_g \omega_g e^{\mathrm{j}\phi_g} e^{\mathrm{j}\omega_g t} \\ -\frac{1}{2} k_m e_p e^{\mathrm{j}\phi_p} e^{\mathrm{j}\omega_p t} + \frac{1}{2} k_m e_p e^{\mathrm{j}\phi_p} e^{\mathrm{j}\omega_p t} - \frac{1}{2} k_m e_p e^{-\mathrm{j}\phi_p} e^{-\mathrm{j}\omega_p t} - \frac{1}{2} k_m e_p e^{-\mathrm{j}\phi_p} e^{-\mathrm{j}\omega_p t} \\ + \frac{1}{2} k_m e_g e^{\mathrm{j}\phi_g} e^{\mathrm{j}\omega_g t} + \frac{1}{2} k_m e_g e^{\mathrm{j}\phi_g} e^{\mathrm{j}\omega_g t} + \frac{1}{2} k_m e_g e^{-\mathrm{j}\phi_g} e^{-\mathrm{j}\omega_g t} - \frac{1}{2} k_m e_g e^{-\mathrm{j}\phi_g} e^{-\mathrm{j}\omega_g t} \\ m_2 e_g \omega_g^2 e^{\mathrm{j}\phi_g} e^{\mathrm{j}\omega_g t} - \mathrm{j} c_m e_p \omega_p e^{-\mathrm{j}\phi_p} e^{-\mathrm{j}\omega_p t} - \mathrm{j} c_m e_g \omega_g e^{\mathrm{j}\phi_g} e^{\mathrm{j}\omega_g t} \\ \frac{1}{2} k_m e_p e^{\mathrm{j}\phi_p} e^{\mathrm{j}\omega_p t} - \frac{1}{2} k_m e_p e^{\mathrm{j}\phi_p} e^{\mathrm{j}\omega_p t} + \frac{1}{2} k_m e_p e^{-\mathrm{j}\phi_p} e^{-\mathrm{j}\omega_p t} + \frac{1}{2} k_m e_p e^{-\mathrm{j}\phi_p} e^{-\mathrm{j}\omega_p t} \\ -\frac{1}{2} k_m e_g e^{\mathrm{j}\phi_g} e^{\mathrm{j}\omega_g t} - \frac{1}{2} k_m e_g e^{\mathrm{j}\phi_g} e^{\mathrm{j}\omega_g t} - \frac{1}{2} k_m e_g e^{-\mathrm{j}\phi_g} e^{-\mathrm{j}\omega_g t} + \frac{1}{2} k_m e_g e^{-\mathrm{j}\phi_g} e^{-\mathrm{j}\omega_g t} \end{array} \right\} \\
&+ \left\{ \begin{array}{c} \frac{c_{s1}}{2\mathrm{j}} e_p \omega_p e^{\mathrm{j}\phi_p} e^{\mathrm{j}\omega_p t} - \frac{c_{s1}}{2\mathrm{j}} e_p \omega_p e^{-\mathrm{j}\phi_p} e^{-\mathrm{j}\omega_p t} - \frac{c_{s1}}{2\mathrm{j}} e_p \omega_p e^{\mathrm{j}\phi_p} e^{\mathrm{j}\omega_p t} - \frac{c_{s1}}{2\mathrm{j}} e_p \omega_p e^{-\mathrm{j}\phi_p} e^{-\mathrm{j}\omega_p t} \\ \frac{c_{s2}}{2\mathrm{j}} e_g \omega_g e^{\mathrm{j}\phi_g} e^{\mathrm{j}\omega_g t} - \frac{c_{s2}}{2\mathrm{j}} e_g \omega_g e^{-\mathrm{j}\phi_g} e^{-\mathrm{j}\omega_g t} + \frac{c_{s2}}{2\mathrm{j}} e_g \omega_g e^{\mathrm{j}\phi_g} e^{\mathrm{j}\omega_g t} + \frac{c_{s2}}{2\mathrm{j}} e_g \omega_g e^{-\mathrm{j}\phi_g} e^{-\mathrm{j}\omega_g t} \end{array} \right\} \\
&+ \left\{ \begin{array}{c} -\frac{k_{s1}}{2} e_p e^{\mathrm{j}\phi_p} e^{\mathrm{j}\omega_p t} - \frac{k_{s1}}{2} e_p e^{-\mathrm{j}\phi_p} e^{-\mathrm{j}\omega_p t} + \frac{k_{s1}}{2} e_p e^{\mathrm{j}\phi_p} e^{\mathrm{j}\omega_p t} - \frac{k_{s1}}{2} e_p e^{-\mathrm{j}\phi_p} e^{-\mathrm{j}\omega_p t} \\ -\frac{k_{s2}}{2} e_g e^{\mathrm{j}\phi g} e^{\mathrm{j}\omega_g t} - \frac{k_{s2}}{2} e_g e^{-\mathrm{j}\phi g} e^{-\mathrm{j}\omega_g t} - \frac{k_{s2}}{2} e_g e^{\mathrm{j}\phi g} e^{\mathrm{j}\omega_g t} + \frac{k_{s2}}{2} e_g e^{-\mathrm{j}\phi g} e^{-\mathrm{j}\omega_g t} \end{array} \right\} \\
&+ \sum_{i=1}^{n} \frac{i\omega_e c_m}{2} \left\{ \begin{array}{c} (e_{xi} e^{\mathrm{j}(\phi_{e_{xi}})} + \mathrm{j} e_{yi} e^{\mathrm{j}(\phi_{e_{yi}})}) e^{\mathrm{j}(i\omega_e t)} + (e_{xi} e^{-\mathrm{j}(\phi_{e_{xi}})} + \mathrm{j} e_{yi} e^{-\mathrm{j}(\phi_{e_{yi}})}) e^{-\mathrm{j}(i\omega_e t)} \\ -(e_{xi} e^{\mathrm{j}(\phi_{e_{xi}})} + \mathrm{j} e_{yi} e^{\mathrm{j}(\phi_{e_{yi}})}) e^{\mathrm{j}(i\omega_e t)} - (e_{xi} e^{-\mathrm{j}(\phi_{e_{xi}})} + j e_{yi} e^{-\mathrm{j}(\phi_{e_{yi}})}) e^{-\mathrm{j}(i\omega_e t)} \end{array} \right\} \\
&+ \frac{k_m}{2} \sum_{i=1}^{n} \left\{ \begin{array}{c} (-\mathrm{j} e_{xi} e^{\mathrm{j}(\phi_{e_{xi}})} + e_{yi} e^{\mathrm{j}(\phi_{e_{yi}})}) e^{\mathrm{j}(i\omega_e t)} + (\mathrm{j} e_{xi} e^{-\mathrm{j}(\phi_{e_{xi}})} - e_{yi} e^{-\mathrm{j}(\phi_{e_{yi}})}) e^{-\mathrm{j}(i\omega_e t)} \\ (\mathrm{j} e_{xi} e^{\mathrm{j}(\phi_{e_{xi}})} - e_{yi} e^{\mathrm{j}(\phi_{e_{yi}})}) e^{\mathrm{j}(i\omega_e t)} + (-\mathrm{j} e_{xi} e^{-\mathrm{j}(\phi_{e_{xi}})} + e_{yi} e^{-\mathrm{j}(\phi_{e_{yi}})}) e^{-\mathrm{j}(i\omega_e t)} \end{array} \right\}
\end{aligned}
\tag{A-15}
$$

Excitations at various frequency components are divided into the forward and backward whirls, by regrouping the coefficients as per its whirl components, to get

$$
\begin{aligned}
\mathbf{f}_r(t) = & \left\{ \begin{array}{c} (k_m e_m) + \mathrm{j}(-m_1 g + k_m e_m) \\ (-k_m e_m) + \mathrm{j}(-m_2 g - k_m e_m) \end{array} \right\} + \left\{ \begin{array}{c} 0 \\ 0 \end{array} \right\} e^{\mathrm{j}\omega_p t} \\
& + \left\{ \begin{array}{c} (m_1 e_p \omega_p^2 e^{-\mathrm{j}\phi_p} - k_m e_p e^{-\mathrm{j}\phi_p}) + \mathrm{j}(c_m e_p \omega_p e^{-\mathrm{j}\phi_p} + c_{s1} e_p e^{-\mathrm{j}\phi_p}) - k_{s1} e_p e^{-\mathrm{j}\phi_p} \\ k_m e_p e^{-\mathrm{j}\phi_p} - \mathrm{j}(c_m e_p \omega_p e^{-\mathrm{j}\phi_p}) \end{array} \right\} e^{-\mathrm{j}\omega_p t} \\
& + \left\{ \begin{array}{c} k_m e_g e^{\mathrm{j}\phi_g} + \mathrm{j}(c_m e_g \omega_g e^{\mathrm{j}\phi_g}) \\ (m_2 e_g \omega_g^2 e^{\mathrm{j}\phi_g} - k_m e_g e^{\mathrm{j}\phi_g}) - \mathrm{j}(c_m e_g \omega_g e^{\mathrm{j}\phi_g} + c_{s2} e_g \omega_g e^{\mathrm{j}\phi_g}) - k_{s2} e_g e^{\mathrm{j}\phi_g} \end{array} \right\} e^{\mathrm{j}\omega_g t} + \left\{ \begin{array}{c} 0 \\ 0 \end{array} \right\} e^{-\mathrm{j}\omega_g t} \\
& + \sum_{i=1}^{n} \left\{ \begin{array}{c} \frac{i\omega_e c_m}{2} (e_{xi} e^{\mathrm{j}(\phi_{e_{xi}})} + \mathrm{j} e_{yi} e^{\mathrm{j}(\phi_{e_{yi}})}) + \frac{k_m}{2} (-\mathrm{j} e_{xi} e^{\mathrm{j}(\phi_{e_{xi}})} + e_{yi} e^{\mathrm{j}(\phi_{e_{yi}})}) \\ -\frac{i\omega_e c_m}{2} (e_{xi} e^{\mathrm{j}(\phi_{e_{xi}})} + \mathrm{j} e_{yi} e^{\mathrm{j}(\phi_{e_{yi}})}) - \frac{k_m}{2} (-\mathrm{j} e_{xi} e^{\mathrm{j}(\phi_{e_{xi}})} + e_{yi} e^{\mathrm{j}(\phi_{e_{yi}})}) \end{array} \right\} e^{\mathrm{j}(i\omega_e t)} \\
& + \sum_{i=1}^{n} \left\{ \begin{array}{c} \frac{i\omega_e c_m}{2} (e_{xi} e^{-\mathrm{j}(\phi_{e_{xi}})} + \mathrm{j} e_{iy} e^{-\mathrm{j}(\phi_{e_{yi}})}) - (-\mathrm{j} e_{xi} e^{-\mathrm{j}(\phi_{e_{xi}})} + e_{yi} e^{-\mathrm{j}(\phi_{e_{yi}})}) \\ -\frac{i\omega_e c_m}{2} (e_{xi} e^{-\mathrm{j}(\phi_{e_{xi}})} + \mathrm{j} e_{yi} e^{-\mathrm{j}(\phi_{e_{yi}})}) + \frac{k_m}{2} (-\mathrm{j} e_{xi} e^{-\mathrm{j}(\phi_{e_{xi}})} + e_{yi} e^{-\mathrm{j}(\phi_{e_{yi}})}) \end{array} \right\} e^{-\mathrm{j}(i\omega_e t)}
\end{aligned} \tag{A-16}
$$

The static, and the forward and backward whirl components are present in Eqn. (A-16). For the simplicity, the static components of force vector are expressed, as,

$$S_1 = S_{1r} + jS_{1j} = (k_m e_m) + \mathrm{j}(-m_1 g + k_m e_m) \tag{A-17}$$

$$S_2 = S_{2r} + jS_{2j} = (-k_m e_m) + \mathrm{j}(-m_2 g - k_m e_m) \tag{A-18}$$

For input shaft, we get

$$R_{f_{e1}} = R_{f_{e1r}} + \mathrm{j}R_{f_{e1j}} = + \sum_{i=1}^{n} \left\{ \frac{i\omega_e c_m}{2} (e_{xi} e^{\mathrm{j}(\phi_{e_{xi}})} + \mathrm{j} e_{yi} e^{\mathrm{j}(\phi_{e_{yi}})}) + \frac{k_m}{2} (-\mathrm{j} e_{xi} e^{\mathrm{j}(\phi_{e_{xi}})} + e_{yi} e^{\mathrm{j}(\phi_{e_{yi}})}) \right\} \tag{A-19}$$

On separating the real and imaginary components, we can write

$$
\begin{aligned}
R_{f_{e1r}} &= \sum_{i=1}^{n} \frac{i\omega_e c_m}{2} \left\{ e_{xi} \cos\phi_{e_{xi}} - e_{yi} sin\phi_{e_{yi}} \right\} + \frac{k_m}{2} \left\{ e_{xi} \sin\phi_{e_{xi}} + e_{yi} \cos\phi_{e_{yi}} \right\}; \\
R_{f_{e1j}} &= \sum_{i=1}^{n} \frac{i\omega_e c_m}{2} \left\{ e_{xi} sin\phi_{e_{xi}} + e_y \cos\phi_{e_{yi}} \right\} - \frac{k_m}{2} \left\{ e_{xi} \cos\phi_{e_{xi}} - e_{yi} sin\phi_{e_{yi}} \right\}
\end{aligned} \tag{A-20}
$$

Similarly, for output shaft, we get

$$R_{f_{e2}} = R_{f_{e2r}} + \mathrm{j}R_{f_{e2j}} = + \sum_{i=1}^{n} \left\{ -\frac{i\omega_e c_m}{2} (e_{xi} e^{\mathrm{j}(\phi_{e_{xi}})} + \mathrm{j} e_{yi} e^{\mathrm{j}(\phi_{e_{yi}})}) + \frac{k_m}{2} (\mathrm{j} e_{xi} e^{\mathrm{j}(\phi_{e_{xi}})} - e_{yi} e^{\mathrm{j}(\phi_{e_{yi}})}) \right\} \tag{A-21}$$

On separating the real and imaginary components, we can write

$$
\begin{aligned}
R_{f_{e2r}} &= -\sum_{i=1}^{n} \frac{i\omega_e c_m}{2} \left\{ e_{xi} \cos\phi_{e_{xi}} - e_{yi} sin\phi_{e_{yi}} \right\} - \frac{k_m}{2} \left\{ e_{xi} \sin\phi_{e_{xi}} + e_{yi} \cos\phi_{e_{yi}} \right\}; \\
R_{f_{e2j}} &= -\sum_{i=1}^{n} \frac{i\omega_e c_m}{2} \left\{ e_{xi} sin\phi_{e_{xi}} + e_y \cos\phi_{e_{yi}} \right\} + \frac{k_m}{2} \left\{ e_{xi} \cos\phi_{e_{xi}} - e_{yi} sin\phi_{e_{yi}} \right\}
\end{aligned} \tag{A-22}
$$

where subscripts: f signifies the forward whirl, r signifies the real part and j signifies the imaginary part.
In the same way, for the backward whirl of the gear mesh frequency, we have
For the input shaft, we define

$$R_{b_{e1}} = R_{b_e 1r} + \mathrm{j}R_{b_e 1j} = \sum_{i=1}^{n} \left\{ \frac{i\omega_e c_m}{2} (e_{xi} e^{-\mathrm{j}(\phi_{e_{xi}})} + \mathrm{j} e_{yi} e^{-\mathrm{j}(\phi_{e_{yi}})}) - (-\mathrm{j} e_{xi} e^{-\mathrm{j}(\phi_{e_{xi}})} + e_{yi} e^{-\mathrm{j}(\phi_{e_{yi}})}) \right\} \tag{A-23}$$

On separating the real and imaginary components, we can write

$$\begin{aligned} R_{b_e1r} &= \sum_{i=1}^{n} \frac{i\omega_e c_m}{2} \left\{ e_{xi} \cos \phi_{e_{xi}} + e_{yi} sin\phi_{e_{yi}} \right\} + \tfrac{k_m}{2} \left\{ e_{xi} \sin \phi_{e_{xi}} - e_{yi} \cos \phi_{e_{yi}} \right\}; \\ R_{b_e1j} &= \sum_{i=1}^{n} \frac{i\omega_e c_m}{2} \left\{ -e_{xi} sin\phi_{e_{xi}} + e_{yi} \cos \phi_{e_{yi}} \right\} + \tfrac{k_m}{2} \left\{ e_{xi} \cos \phi_{e_{xi}} + e_{yi} sin\phi_{e_{yi}} \right\} \end{aligned} \tag{A-24}$$

For the output shaft, we define

$$R_{b_{e2}} = R_{b_e2r} + \mathrm{j}R_{b_e2j} = \sum_{i=1}^{n} \left\{ -\frac{i\omega_e c_m}{2} \left(e_{xi} e^{-\mathrm{j}(\phi_{e_{xi}})} + \mathrm{j}e_{yi} e^{-\mathrm{j}(\phi_{e_{yi}})} \right) - \frac{k_m}{2} \left(\mathrm{j}e_{xi} e^{-\mathrm{j}(\phi_{e_{xi}})} - e_{yi} e^{-\mathrm{j}(\phi_{e_{yi}})} \right) \right\} \tag{A-25}$$

On separating the real and imaginary components, we can write

$$\begin{aligned} R_{b_e2r} &= -\sum_{i=1}^{n} \frac{i\omega_e c_m}{2} \left\{ e_{xi} \cos \phi_{e_{xi}} + e_{yi} sin\phi_{e_{yi}} \right\} - \tfrac{k_m}{2} \left\{ e_{xi} \sin \phi_{e_{xi}} - e_{yi} \cos \phi_{e_{yi}} \right\}; \\ R_{b_e2j} &= -\sum_{i=1}^{n} \frac{i\omega_e c_m}{2} \left\{ -e_{xi} sin\phi_{e_{xi}} + e_{yi} \cos \phi_{e_{yi}} \right\} - \tfrac{k_m}{2} \left\{ e_{xi} \cos \phi_{e_{xi}} + e_{yi} sin\phi_{e_{yi}} \right\} \end{aligned} \tag{A-26}$$

where $\begin{matrix} R_{f_e r} = e_{xi} \cos \phi_{e_{xi}} - e_{yi} sin\phi_{e_{yi}}; & R_{f_e j} = e_{xi} sin\phi_{e_{xi}} + e_y \cos \phi_{e_{yi}} \\ R_{b_e r} = e_{xi} \cos \phi_{e_{xi}} + e_{yi} \sin \phi_{e_{yi}}; & R_{b_e j} = -e_{xi} \sin \phi_{e_{xi}} + e_{yi} \cos \phi_{e_{yi}} \end{matrix}$

where subscript b signifies the backward whirl, r signifies the real part and j signifies the imaginary part. As there are no forward whirl components of pinion runout frequency component, we can write from Eqn. (A-16)

$$R_{f_{p1}} = 0; \quad R_{f_{p2}} = 0 \tag{A-27}$$

Similarly, the pinion backward whirl runout frequency component is written as,

$$R_{b_{p1}} = R_{b_{p1r}} + \mathrm{j}R_{b_{p1j}} = (m_1 e_p \omega_p^2 - k_m e_p - k_{s1} e_p) e^{-\mathrm{j}\phi_p} + \mathrm{j}(c_m e_p \omega_p + c_{s1} e_p) e^{-\mathrm{j}\phi_p} \tag{A-28}$$

$$R_{b_{p2}} = R_{b_{p2r}} + \mathrm{j}R_{b_{p2j}} = k_m e_p e^{-\mathrm{j}\phi_p} - \mathrm{j}c_m e_p \omega_p e^{-\mathrm{j}\phi_p} \tag{A-29}$$

The real and imaginary terms, for the input shaft, are written as

$$R_{b_{p1r}} = (m_1 e_p \omega_p^2 - k_m e_p - k_{s1} e_p) \cos \phi_p + (c_m e_p \omega_p + c_{s1} e_p \omega_p) \sin \phi_p \tag{A-30}$$

$$R_{b_{p1j}} = (c_m e_p \omega_p + c_{s1} e_p \omega_p) \cos \phi_p + (-m_1 e_p \omega_p^2 + k_m e_p + k_{s1}) \sin \phi_p \tag{A-31}$$

Similarly, the real and imaginary parts, for the output shaft, are written as

$$R_{b_{p2r}} = (k_m e_p) \cos \phi_p - (c_m e_p \omega_p) \sin \phi_p \tag{A-32}$$

$$R_{b_{p2j}} = (-c_m e_p \omega_p) \cos \phi_p - (k_m e_p) \sin \phi_p \tag{A-33}$$

The gear forward whirl runout frequency component is written as,

$$R_{f_{g1}} = R_{f_{g1r}} + \mathrm{j}R_{f_{g1j}} = (k_m e_g) e^{\mathrm{j}\phi_g} - \mathrm{j}(-c_m e_g \omega_g) e^{\mathrm{j}\phi_g} \tag{A-34}$$

The real and imaginary terms, for input shaft, are written as,

$$R_{f_{g1r}} = k_m e_g \cos \phi_g - (c_m e_g \omega_g) \sin \phi_g \tag{A-35}$$

$$R_{f_{g1j}} = (c_m e_g \omega_g) \cos \phi_g + k_m e_g \sin \phi_g \tag{A-36}$$

Similarly, for the output shaft the forward whirl gear runout frequency components is written as,

$$R_{f_{g2}} = R_{f_{g2r}} + \mathrm{j}R_{f_{g2j}} = (m_2 e_g \omega_g^2 - k_m e_g - k_{s2} e_g) e^{\mathrm{j}\phi_g} - \mathrm{j}(c_m e_g \omega_g + c_{s2} e_g \omega_g) e^{\mathrm{j}\phi_g} \tag{A-37}$$

On separating the real and imaginary parts, we get

$$R_{f_{g2r}} = (m_2 e_g \omega_g^2 - k_m e_g - k_{s2} e_g) \cos\phi_g + (c_m e_g \omega_g + c_{s2} e_g \omega_g) \sin\phi_g \tag{A-38}$$

and

$$R_{f_{g2j}} = (-c_m e_g \omega_g - c_{s2} e_g \omega_g) \cos\phi_g + (m_2 e_g \omega_g^2 - k_m e_g - k_{s2} e_g) \sin\phi_g \tag{A-39}$$

As there is no backward whirl of the gear runout frequency, so we can write

$$R_{b_{g1}} = 0; \qquad R_{b_{g2}} = 0 \tag{A-40}$$

Appendix B. Grouping of the forward and backward whirl components

Similar frequency components are collected and expressed them in frequency domain for the static, forward and backward whirl components, as follows

$$S_{1r} = k_m e_m; \qquad S_{1j} = -m_1 g + k_m e_m; \qquad S_{2r} = -k_m e_m; \qquad S_{2j} = -m_2 g - k_m e_m \tag{A-41}$$

$$\begin{aligned} S_{f_{e1r}} &= (i\omega_e c_m R_{f_{er}} + k_m R_{f_{ej}})/2; & S_{f_{e1j}} &= (i\omega_e c_m R_{f_{ej}} - k_m R_{f_{er}})/2; \\ S_{f_{e2r}} &= (-i\omega_e c_m R_{f_{er}} - k_m R_{f_{ej}})/2; & S_{f_{e2j}} &= (-i\omega_e c_m R_{f_{ej}} + k_m R_{f_{er}})/2 \end{aligned} \tag{A-42}$$

$$\begin{aligned} S_{b_{e1r}} &= (i\omega_e c_m R_{b_{er}} - k_m R_{b_{ej}})/2; & S_{b_{e1j}} &= (i\omega_e c_m R_{b_{ej}} + k_m R_{b_{er}})/2; \\ S_{b_{e2r}} &= (-i\omega_e c_m R_{b_{er}} + k_m R_{b_{ej}})/2; & S_{b_{e2j}} &= (-i\omega_e c_m R_{b_{ej}} - k_m R_{b_{er}})/2 \end{aligned} \tag{A-43}$$

On substituting Eqns. (A-41) to (A-43) in Eqn. (15), we get the force vector as,

$$\begin{aligned} \mathbf{f}_r = &\begin{Bmatrix} S_{1r} + \mathrm{j}S_{1j} \\ S_{2r} + \mathrm{j}S_{2j} \end{Bmatrix} + \begin{Bmatrix} R_{f_{p1r}} + \mathrm{j}R_{f_{p1j}} \\ R_{f_{p2r}} + \mathrm{j}R_{f_{p2j}} \end{Bmatrix} e^{\mathrm{j}\omega_p t} + \begin{Bmatrix} R_{b_{p1r}} + \mathrm{j}R_{b_{p1j}} \\ R_{b_{p2r}} + \mathrm{j}R_{b_{p2j}} \end{Bmatrix} e^{-\mathrm{j}\omega_p t} + \begin{Bmatrix} R_{f_{g1r}} + \mathrm{j}R_{f_{g1j}} \\ R_{f_{g2r}} + \mathrm{j}R_{f_{g2j}} \end{Bmatrix} e^{\mathrm{j}\omega_g t} \\ &+ \begin{Bmatrix} R_{b_{g1r}} + \mathrm{j}R_{b_{g1j}} \\ R_{b_{g2r}} + \mathrm{j}R_{b_{g2j}} \end{Bmatrix} e^{-\mathrm{j}\omega_g t} + \sum_{i=1}^{n} \left(\begin{Bmatrix} S_{f_{e1r}} + jS_{f_{e1j}} \\ S_{f_{e2r}} + jS_{f_{e2j}} \end{Bmatrix} e^{j(i\omega_e t)} + \begin{Bmatrix} S_{b_{e1r}} + jS_{b_{e1j}} \\ S_{b_{e2r}} + jS_{b_{e2j}} \end{Bmatrix} e^{-j(i\omega_e t)} \right) \end{aligned} \tag{A-44}$$

On substituting forces from Eqn. (A-10) to Eqn. (A-11) and Eqn. (A-44) into Eqn. (11), equations of motion in a matrix form is written as,

$$\begin{aligned} &\begin{bmatrix} m_1 & 0 \\ 0 & m_2 \end{bmatrix} \begin{Bmatrix} \ddot{r}_1 \\ \ddot{r}_2 \end{Bmatrix} + \begin{bmatrix} c_{s1} + c_m & -c_m \\ -c_m & c_{s2} + c_m \end{bmatrix} \begin{Bmatrix} \dot{r}_1 \\ \dot{r}_2 \end{Bmatrix} + \begin{bmatrix} k_{s1} + k_m & -k_m \\ -k_m & k_{s2} + k_m \end{bmatrix} \begin{Bmatrix} r_1 \\ r_2 \end{Bmatrix} = \\ &\begin{Bmatrix} S_1 \\ S_2 \end{Bmatrix} + \begin{Bmatrix} R_{f_{p1r}} + \mathrm{j}R_{f_{p1j}} \\ R_{f_{p2r}} + \mathrm{j}R_{f_{p2j}} \end{Bmatrix} e^{\mathrm{j}\omega_p t} + \begin{Bmatrix} R_{b_{p1r}} + \mathrm{j}R_{b_{p1j}} \\ R_{b_{p2r}} + \mathrm{j}R_{b_{p2j}} \end{Bmatrix} e^{-\mathrm{j}\omega_p t} + \begin{Bmatrix} R_{f_{g1r}} + \mathrm{j}R_{f_{g1j}} \\ R_{f_{g2r}} + \mathrm{j}R_{f_{g2j}} \end{Bmatrix} e^{\mathrm{j}\omega_g t} + \\ &\begin{Bmatrix} R_{b_{g1r}} + \mathrm{j}R_{b_{g1j}} \\ R_{b_{g2r}} + \mathrm{j}R_{b_{g2j}} \end{Bmatrix} e^{-\mathrm{j}\omega_g t} + \sum_{i=1}^{n} \left(\begin{Bmatrix} S_{f_{e1r}} + \mathrm{j}S_{f_{e1j}} \\ S_{f_{e2r}} + \mathrm{j}S_{f_{e2j}} \end{Bmatrix} e^{\mathrm{j}(i\omega_e t)} + \begin{Bmatrix} S_{b_{e1r}} + \mathrm{j}S_{b_{e1j}} \\ S_{b_{e2r}} + \mathrm{j}S_{b_{e2j}} \end{Bmatrix} e^{-\mathrm{j}(i\omega_e t)} \right) \end{aligned} \tag{A-45}$$

Here S, $S_{f_{er}}$, $S_{f_{ej}}$, $S_{b_{er}}$ and $S_{b_{ej}}$ contains the TE amplitude and phase of the gear mesh, i signifies harmonics of gear order and n represents number of harmonics considered in the TE. For presumed value of TE and its variable components, Eqn. (A-45) can be solved to get the response of the geared-rotor system. Since equations of motion are linear, assumed solution for each harmonic can be added up using the principle of superposition, as

For i^{th} harmonic, Eqn. (A-45) can be written as,

$$m_1\ddot{r}_1 + (c_{s1} + c_m)\dot{r}_1 - c_m\dot{r}_2 + (k_{s1} + k_m)r_1 - k_m r_2 = S_1 + S_{f_{e1}}e^{j(i\omega_e t)} + S_{b_{e1}}e^{-j(i\omega_e t)} + R_{f_{p1}}e^{j\omega_p t} + R_{f_{p1}}e^{-j\omega_p t} + R_{f_{g1}}e^{j\omega_g t} + R_{f_{g1}}e^{-j\omega_g t} \tag{A-46}$$

and

$$m_2\ddot{r}_2 + (c_{s2} + c_m)\dot{r}_2 - c_m\dot{r}_1 + (k_{s2} + k_m)r_2 - k_m r_1 = S_2 - S_{f_{e2}}e^{j(i\omega_e t)} - S_{b_{e2}}e^{-j(i\omega_e t)} + R_{f_{p2}}e^{j\omega_p t} + R_{f_{p2}}e^{-j\omega_p t} + R_{f_{g2}}e^{j\omega_g t} + R_{f_{g2}}e^{-j\omega_g t} \tag{A-47}$$

with

$$S_1 = (k_m e_m) + j(-m_1 g + k_m e_m); \qquad S_2 = -(k_m e_m) + j(-m_2 g - k_m e_m) \tag{A-48}$$

and

$$\begin{aligned} S_{f_{e1}} &= S_{f_{e1r}} + jS_{f_{e1j}}; \qquad S_{b_{e1}} = S_{b_{e1r}} + jS_{b_{e1j}}; \\ S_{f_{e2}} &= S_{f_{e2r}} + jS_{f_{e2j}}; \qquad S_{b_{e2}} = S_{b_{e2r}} + jS_{b_{e2j}} \end{aligned} \tag{A-49}$$

where S_1 and S_2 are the static components, and $S_{f_{e1}}$, $S_{b_{e1}}$, $S_{f_{e2}}$ and $S_{b_{e2}}$ are the fluctuating components with harmonics of gear mesh frequency. Herein, f and b subscripts signify the forward and backward whirls.

From Eqn. (A-46) and (A-47), we can write

Only the static force, it will give

$$(k_{s1} + k_m)r_1 - k_m r_2 = S_1; \quad (k_{s2} + k_m)r_2 - k_m r_1 = S_2 \tag{A-50}$$

For the forward whirl force, we have

$$m_1\ddot{r}_1 + (c_{s1} + c_m)\dot{r}_1 - c_m\dot{r}_2 + (k_{s1} + k_m)r_1 - k_m r_2 = (S_{f_{e1r}} + jS_{f_{e1j}})e^{j(i\omega_e t)} + (R_{f_{p1r}} + jR_{f_{p1j}})e^{j\omega_p t} + (R_{f_{g1r}} + jR_{f_{g1j}})e^{j\omega_g t} \tag{A-51}$$

and

$$m_2\ddot{r}_2 + (c_{s2} + c_m)\dot{r}_2 - c_m\dot{r}_1 + (k_{s2} + k_m)r_2 - k_m r_1 = (S_{f_{e2r}} + jS_{f_{e2j}})e^{j(i\omega_e t)} + (R_{f_{p2r}} + jR_{f_{p2j}})e^{j\omega_p t} + (R_{f_{g2r}} + jR_{f_{g2j}})e^{j\omega_g t} \tag{A-52}$$

For the backward whirl force, we have

$$m_1\ddot{r}_1 + (c_{s1} + c_m)\dot{r}_1 - c_m\dot{r}_2 + (k_{s1} + k_m)r_1 - k_m r_2 = (S_{b1r} + jS_{b1j})e^{-j(i\omega_e t)} + (R_{b_{p1r}} + jR_{b_{p1j}})e^{-j\omega_p t} + (R_{b_{g1r}} + jR_{b_{g1j}})e^{-j\omega_g t} \tag{A-53}$$

and

$$m_2\ddot{r}_2 + (c_{s2} + c_m)\dot{r}_2 - c_m\dot{r}_1 + (k_{s2} + k_m)r_2 - k_m r_1 = (S_{b2r} + jS_{b2j})e^{-j(i\omega_e t)} + (R_{b_{p2r}} + jR_{b_{p2j}})e^{-j\omega_p t} + (R_{b_{g2r}} + jR_{b_{g2j}})e^{-j\omega_g t} \tag{A-54}$$

Assuming a solution due to the static force for Eqn. (A-50), as

$$r_1 = P_{s1} = P_{s1r} + jP_{s1j} \qquad \text{and} \qquad r_2 = P_{s2} = P_{s1r} + jP_{s1j} \tag{A-55}$$

where P_{s1} and P_{s2} are in complex form as $P_s = P_{sr} + jP_{sj}$. Presuming the forward whirl solution for Eqns. (A-51) and (A-52), as

$$r_1(t) = P_{f_{e1}}e^{j(i\omega_e t)} + P_{f_{p1}}e^{j(i\omega_p t)} + P_{f_{g1}}e^{j(i\omega_g t)}$$

and

$$r_2(t) = P_{f_{e2}} e^{\mathrm{j}(i\omega_e t)} + P_{f_{p2}} e^{\mathrm{j}(i\omega_p t)} + P_{f_{g2}} e^{\mathrm{j}(i\omega_g t)} \tag{A-56}$$

where P_{f1} and P_{f2} are in the complex form as $P_f = P_{fr} + jP_{fj}$. Presuming the backward whirl solution for Eqns. (A-53) and (A-54), as

$$r_1(t) = P_{b_e 1} e^{-\mathrm{j}(i\omega_e t)} + P_{b_p 1} e^{-\mathrm{j}(i\omega_p t)} + P_{b_g 1} e^{-\mathrm{j}(i\omega_g t)}$$

and

$$r_2(t) = P_{b_e 2} e^{-\mathrm{j}(i\omega_e t)} + P_{b_p 2} e^{-\mathrm{j}(i\omega_p t)} + P_{b_g 2} e^{-\mathrm{j}(i\omega_g t)} \tag{A-57}$$

where P_b is in complex form as $P_b = P_{br} + jP_{bj}$. On substituting back Eqn. (A-57) into Eqn. (A-50), we get

For the static force, we get

$$(k_{s1} + k_m)P_{s1} - k_m P_{s2} = S_1; \qquad (k_{s2} + k_m)P_{s2} - k_m P_{s1} = S_2 \tag{A-58}$$

Now, Eqn. (A-58) can be arranged in the real and imaginary parts, as

$$(k_{s1} + k_m)(P_{s1r} + \mathrm{j}P_{s1j}) - k_m(P_{s2r} + \mathrm{j}P_{s2j}) = S_{1r} + \mathrm{j}S_{1j} \tag{A-59}$$

and

$$(k_{s2} + k_m)(P_{s2r} + \mathrm{j}P_{s2j}) - k_m(P_{s1r} + \mathrm{j}P_{s1j}) = S_{2r} + \mathrm{j}S_{2j} \tag{A-60}$$

Both sides of Eqns. (A-59) and (A-60) by extraction the real and imaginary parts, to get the static force real and imaginary parts, as

$$(k_{s1} + k_m)P_{s1r} - k_m P_{s2r} = S_{1r}; \qquad -k_m P_{s1r} + (k_{s2} + k_m)P_{s2r} = S_{2r} \tag{A-61}$$

and

$$(k_{s1} + k_m)P_{s1j} - k_m P_{s2j} = S_{1j}; \qquad -k_m P_{s1j} + (k_{s2} + k_m)P_{s2j} = S_{2j} \tag{A-62}$$

On combining Eqns. (A-61) and (A-62), we get

$$\mathbf{A}_s \mathbf{p}_s = \mathbf{s}_s \tag{A-63}$$

with

$$\mathbf{A}_{si} = \begin{bmatrix} k_{s1} + k_m & 0 & -k_m & 0 \\ 0 & k_{s1} + k_m & 0 & -k_m \\ -k_m & 0 & k_{s2} + k_m & 0 \\ 0 & -k_m & 0 & k_{s2} + k_m \end{bmatrix}; \quad \mathbf{p}_s = \begin{Bmatrix} P_{s1r} \\ P_{s1j} \\ P_{s2r} \\ P_{s2j} \end{Bmatrix}; \quad \mathbf{s}_s = \begin{Bmatrix} S_{1r} \\ S_{1j} \\ S_{2r} \\ S_{2j} \end{Bmatrix} \tag{A-64}$$

On substituting back Eqn. (A-56) in Eqns. (A-51) and (A-52), for the forward whirl force, we get

$$-m_1 i^2 \omega_e^2 P_{f_{e1}} + \mathrm{j}i\omega_e(c_{s1} + c_m)P_{f_{e1}} - \mathrm{j}i\omega_e c_m P_{f_{e2}} + (k_{s1} + k_m)P_{f_{e1}} - k_m P_{f_{e2}} = S_{f_{e1}} \tag{A-65}$$

$$-m_1 i^2 \omega_p^2 P_{f_{p1}} + \mathrm{j}i\omega_p(c_{s1} + c_m)P_{f_{p1}} - \mathrm{j}i\omega_p c_m P_{f_{p2}} + (k_{s1} + k_m)P_{f_{p1}} - k_m P_{f_{p2}} = R_{f_{p1}} \tag{A-66}$$

$$-m_1 i^2 \omega_g^2 P_{f_{g1}} + \mathrm{j}i\omega_g(c_{s1} + c_m)P_{f_{g1}} - \mathrm{j}i\omega_g c_m P_{f_{g2}} + (k_{s1} + k_m)P_{f_{g1}} - k_m P_{f_{g2}} = R_{f_{g1}} \tag{A-67}$$

$$-m_2 i^2 \omega_e^2 P_{f_{e2}} + \mathrm{j}i\omega_e(c_{s2} + c_m)P_{f_{e2}} - \mathrm{j}i\omega_e c_m P_{f_{e1}} + (k_{s2} + k_m)P_{f_{e2}} - k_m P_{f_{e1}} = -S_{f_{e2}} \tag{A-68}$$

$$-m_2 i^2 \omega_p^2 P_{f_{p2}} + \mathrm{j}i\omega_p(c_{s2} + c_m)P_{f_{p2}} - \mathrm{j}i\omega_p c_m P_{f_{p1}} + (k_{s2} + k_m)P_{f_{p2}} - k_m P_{f_{p1}} = R_{f_{p2}} \tag{A-69}$$

$$-m_2 i^2 \omega_g^2 P_{f_{g2}} + \mathrm{j}i\omega_g(c_{s2} + c_m)P_{f_{g2}} - \mathrm{j}i\omega_g c_m P_{f_{g1}} + (k_{s2} + k_m)P_{f_{g2}} - k_m P_{f_{g1}} = R_{f_{g2}} \tag{A-70}$$

where $i = 1,2, \cdots, n$.

These are organized into the real and imaginary components, as

$$-m_1 i^2\omega_e^2(P_{f_{e1r}}+\mathrm{j}P_{f_{e1j}})+(\mathrm{j}i\omega_e)(c_{s1}+c_m)(P_{f_{e1r}}+\mathrm{j}P_{f_{e1j}})-(\mathrm{j}i\omega_e)c_m(P_{f_{e2r}}+\mathrm{j}P_{f_{e2j}})+(k_{s1}+k_m)(P_{f_{e1r}}+\mathrm{j}P_{f_{e1j}})-k_m(P_{f_{e2r}}+\mathrm{j}P_{f_{e2j}})=(S_{f_{e1r}}+\mathrm{j}S_{f_{e1j}}) \tag{A-71}$$

$$-m_1 i^2\omega_p^2(P_{f_{p1r}}+jP_{f_{p1j}})+\mathrm{j}i\omega_p(c_{s1}+c_m)(P_{f_{p1r}}+\mathrm{j}P_{f_{p1j}})-\mathrm{j}i\omega_p c_m(P_{f_{p2r}}+\mathrm{j}P_{f_{p2j}})+(k_{s1}+k_m)(P_{f_{p1r}}+\mathrm{j}P_{f_{p1j}})-k_m(P_{f_{p2r}}+\mathrm{j}P_{f_{p2j}})=(R_{f_{p1r}}+\mathrm{j}R_{f_{p1j}}) \tag{A-72}$$

$$-m_1 i^2\omega_g^2(P_{f_{g1r}}+\mathrm{j}P_{f_{g1j}})+\mathrm{j}i\omega_g(c_{s1}+c_m)(P_{f_{g1r}}+\mathrm{j}P_{f_{g1j}})-\mathrm{j}i\omega_g c_m(P_{f_{g2r}}+\mathrm{j}P_{f_{g2j}})+(k_{s1}+k_m)(P_{f_{g1r}}+\mathrm{j}P_{f_{g1j}})-k_m(P_{f_g2r}+\mathrm{j}P_{f_{g2j}})=(R_{f_g1r}+\mathrm{j}R_{f_{g1j}}) \tag{A-73}$$

$$-m_2 i^2\omega_e^2(P_{f_{e2r}}+\mathrm{j}P_{f_{e2j}})+\mathrm{j}i\omega_e(c_{s2}+c_m)(P_{f_{e2r}}+\mathrm{j}P_{f_{e2j}})-\mathrm{j}i\omega_e c_m(P_{f_{e1r}}+\mathrm{j}P_{f_{e1j}})+(k_{s2}+k_m)(P_{f_{e2r}}+\mathrm{j}P_{f_{e2j}})-k_m(P_{f_{e1r}}+\mathrm{j}P_{f_{e1j}})=(S_{f_{e2r}}+\mathrm{j}S_{f_{e2j}}) \tag{A-74}$$

$$-m_2 i^2\omega_p^2(P_{f_{p2r}}+\mathrm{j}P_{f_{p2j}})+\mathrm{j}i\omega_p(c_{s2}+c_m)(P_{f_{p2r}}+\mathrm{j}P_{f_{p2j}})-\mathrm{j}i\omega_p c_m(P_{f_{p1r}}+\mathrm{j}P_{f_{p1j}})+(k_{s2}+k_m)(P_{f_{p2r}}+\mathrm{j}P_{f_{p1j}})-k_m(P_{f_{p1r}}+\mathrm{j}P_{f_{p1j}})=(R_{f_{p2r}}+\mathrm{j}R_{f_{p2j}}) \tag{A-75}$$

$$-m_2 i^2\omega_g^2(P_{f_{g2r}}+\mathrm{j}P_{f_{g2j}})+\mathrm{j}i\omega_g(c_{s2}+c_m)(P_{f_{g2r}}+\mathrm{j}P_{f_{g2j}})-\mathrm{j}i\omega_g c_m(P_{f_{g1r}}+\mathrm{j}P_{f_{g1j}})+(k_{s2}+k_m)(P_{f_{g2r}}+\mathrm{j}P_{f_{g2j}})-k_m(P_{f_{g1r}}+\mathrm{j}P_{f_{g1j}})=(R_{f_{g2r}}+\mathrm{j}R_{f_{g2j}}) \tag{A-76}$$

where $i = 1,2,\cdots,n$

Both sides of Eqns. (A-71) through (A-76) are extracted for the real and imaginary parts, as

Forward whirl real component

$$-m_1 i^2\omega_e^2 P_{f_{e1r}}-i\omega_e(c_{s1}+c_m)P_{f_{e1j}}+i\omega_e c_m P_{f_{e2j}}+(k_{s1}+k_m)P_{f_{e1r}}-k_m P_{f_{e2r}}=S_{f_{e1r}} \tag{A-77}$$

$$-m_1 i^2\omega_p^2 P_{f_{p1r}}-i\omega_p(c_{s1}+c_m)P_{f_{p1j}}+i\omega_p c_m P_{f_{p2j}}+(k_{s1}+k_m)P_{f_{p1r}}-k_m P_{f_{p2r}}=R_{f_{p1r}} \tag{A-78}$$

$$-m_1 i^2\omega_g^2 P_{f_{g1r}}-i\omega_g(c_{s1}+c_m)P_{f_{g1j}}+i\omega_g c_m P_{f_{g2j}}+(k_{s1}+k_m)P_{f_{g1r}}-k_m P_{f_{g2r}}=R_{f_{g1r}} \tag{A-79}$$

$$-m_2 i^2\omega_e^2 P_{f_{e2r}}-i\omega_e(c_{s2}+c_m)P_{f_{e2j}}+i\omega_e c_m P_{f_{e1j}}+(k_{s2}+k_m)P_{f_{e2r}}-k_m P_{f_{e1r}}=S_{f_{e2r}} \tag{A-80}$$

$$-m_2 i^2\omega_p^2 P_{f_{p2r}}-i\omega_p(c_{s2}+c_m)P_{f_{p2j}}+i\omega_p c_m P_{f_{p1j}}+(k_{s2}+k_m)P_{f_{p2r}}-k_m P_{f_{p1r}}=R_{f_{p2r}} \tag{A-81}$$

$$-m_2 i^2\omega_g^2 P_{f_{g2r}}-i\omega_g(c_{s2}+c_m)P_{f_{g3j}}+i\omega_g c_m P_{f_{g1j}}+(k_{s2}+k_m)P_{f_{g2r}}-k_m P_{f_{g1r}}=R_{f_{g2r}} \tag{A-82}$$

Forward whirl imaginary component

$$-m_1 i^2\omega_e^2 P_{f_{e1j}}+i\omega_e(c_{s1}+c_m)P_{f_{e1r}}-i\omega_e c_m P_{f_{e2r}}+(k_{s1}+k_m)P_{f_{e1j}}-k_m P_{f_{e2j}}=S_{f_{e1j}} \tag{A-83}$$

$$-m_1 i^2\omega_p^2 P_{f_{p1j}}+i\omega_p(c_{s1}+c_m)P_{f_{p1r}}-i\omega_p c_m P_{f_{p2r}}+(k_{s1}+k_m)P_{f_{p1j}}-k_m P_{f_{p2j}}=R_{f_{p1j}} \tag{A-84}$$

$$-m_1 i^2\omega_g^2 P_{f_{g1j}}+i\omega_g(c_{s1}+c_m)P_{f_{g1r}}-i\omega_g c_m P_{f_{g2r}}+(k_{s1}+k_m)P_{f_{g1j}}-k_m P_{f_{g2j}}=R_{f_{g1j}} \tag{A-85}$$

$$-m_2 i^2\omega_e^2 P_{f_{e2j}}+i\omega_e(c_{s2}+c_m)P_{f_{e2r}}-i\omega_e c_m P_{f_{e1r}}+(k_{s2}+k_m)P_{f_{e2j}}-k_m P_{f_{e1j}}=S_{f_{e2j}} \tag{A-86}$$

$$-m_2 i^2\omega_p^2 P_{f_{p2j}}+i\omega_p(c_{s2}+c_m)P_{f_{p2r}}-i\omega_p c_m P_{f_{p1r}}+(k_{s2}+k_m)P_{f_{p2j}}-k_m P_{f_{p1j}}=R_{f_{p2j}} \tag{A-87}$$

$$-m_2 i^2 \omega_g^2 P_{f_{g2j}} + i\omega_g (c_{s2} + c_m) P_{f_{g2r}} - i\omega_g c_m P_{f_{g1r}} + (k_{s2} + k_m) P_{f_{g2j}} - k_m P_{f_{g1j}} = R_{f_{g2j}} \tag{A-88}$$

On combining Eqns. (A-77) through (A-88), we get

$$\mathbf{A}_{fi} \mathbf{p}_{fi} = \mathbf{s}_{fi} \tag{A-89}$$

$$\mathbf{A}_{fi} = \begin{bmatrix} \mathbf{A}_{f_{ei}} & 0 & 0 \\ 0 & \mathbf{A}_{f_{pi}} & 0 \\ 0 & 0 & \mathbf{A}_{f_{gi}} \end{bmatrix} \tag{A-90}$$

with

$$\mathbf{A}_{f_e i} = \begin{bmatrix} -m_1 i^2 \omega_e^2 + (k_{s1} + k_m) & -i\omega_e (c_{s1} + c_m) & -k_m & i\omega_e c_m \\ i\omega_e (c_{s1} + c_m) & -m_1 i^2 \omega_e^2 + (k_{s1} + k_m) & -i\omega_e c_m & -k_m \\ -k_m & i\omega_e c_m & -m_2 i^2 \omega_e^2 + (k_{s2} + k_m) & -i\omega_e (c_{s2} + c_m) \\ -i\omega_e c_m & -k_m & i\omega_e (c_{s2} + c_m) & -m_2 i^2 \omega_e^2 + (k_{s2} + k_m) \end{bmatrix} \tag{A-91}$$

$$\mathbf{A}_{f_p i} = \begin{bmatrix} -m_1 i^2 \omega_p^2 + (k_{s1} + k_m) & -i\omega_p (c_{s1} + c_m) & -k_m & i\omega_p c_m \\ i\omega_p (c_{s1} + c_m) & -m_1 i^2 \omega_p^2 + (k_{s1} + k_m) & -i\omega_p c_m & -k_m \\ -k_m & i\omega_p c_m & -m_2 i^2 \omega_p^2 + (k_{s2} + k_m) & -i\omega_p (c_{s2} + c_m) \\ -i\omega_p c_m & -k_m & i\omega_p (c_{s2} + c_m) & -m_2 i^2 \omega_p^2 + (k_{s2} + k_m) \end{bmatrix} \tag{A-92}$$

$$\mathbf{A}_{f_g i} = \begin{bmatrix} -m_1 i^2 \omega_g^2 + (k_{s1} + k_m) & -i\omega_g (c_{s1} + c_m) & -k_m & i\omega_g c_m \\ i\omega_g (c_{s1} + c_m) & -m_1 i^2 \omega_g^2 + (k_{s1} + k_m) & -i\omega_g c_m & -k_m \\ -k_m & i\omega_g c_m & -m_2 i^2 \omega_g^2 + (k_{s2} + k_m) & -i\omega_g (c_{s2} + c_m) \\ -i\omega_p c_m & -k_m & i\omega_g (c_{s2} + c_m) & -m_2 i^2 \omega_g^2 + (k_{s2} + k_m) \end{bmatrix} \tag{A-93}$$

On substituting back Eqn. (A-57) in Eqns. (A-53) and (A-54), for the backward whirl force, we get

$$-m_1 i^2 \omega_e^2 P_{b_{e1}} - \mathrm{j} i\omega_e (c_{s1} + c_m) P_{b_{e1}} + \mathrm{j} i\omega_e c_m P_{b_{e2}} + (k_{s1} + k_m) P_{b_{e1}} - k_m P_{b_{e2}} = S_{b_{e1}} \tag{A-94}$$

$$-m_1 i^2 \omega_p^2 P_{b_{p1}} - \mathrm{j} i\omega_p (c_{s1} + c_m) P_{b_{p1}} + \mathrm{j} i\omega_p c_m P_{b_{p2}} + (k_{s1} + k_m) P_{b_{p1}} - k_m P_{b_{p2}} = R_{b_{p1}} \tag{A-95}$$

$$-m_1 i^2 \omega_g^2 P_{b_{g1}} - \mathrm{j} i\omega_g (c_{s1} + c_m) P_{b_{g1}} + \mathrm{j} i\omega_g c_m P_{b_{g2}} + (k_{s1} + k_m) P_{b_{g1}} - k_m P_{b_{g2}} = R_{b_{g1}} \tag{A-96}$$

$$-m_2 i^2 \omega_e^2 P_{b_{e2}} - \mathrm{j} i\omega_e (c_{s2} + c_m) P_{b_{e2}} + \mathrm{j} i\omega_e c_m P_{b_{e1}} + (k_{s2} + k_m) P_{b_{e2}} - k_m P_{b_{e1}} = S_{b_{e2}} \tag{A-97}$$

$$-m_2 i^2 \omega_p^2 P_{b_{p2}} - \mathrm{j} i\omega_p (c_{s2} + c_m) P_{b_{p2}} + \mathrm{j} i\omega_p c_m P_{b_{p1}} + (k_{s2} + k_m) P_{b_{p2}} - k_m P_{b_{p1}} = R_{b_{p2}} \tag{A-98}$$

$$-m_2 i^2 \omega_g^2 P_{b_{g2}} - \mathrm{j} i\omega_g (c_{s2} + c_m) P_{b_{g2}} + \mathrm{j} i\omega_g c_m P_{b_{g1}} + (k_{s2} + k_m) P_{b_{g2}} - k_m P_{b_{g1}} = R_{b_{g2}} \tag{A-99}$$

with $i = 1,2, \cdots, n$

These are organized into the real and imaginary components, as

$$\begin{aligned} &-m_1 i^2 \omega_e^2 (P_{b_{e1r}} + \mathrm{j} P_{b_{e1j}}) - \mathrm{j} i\omega_e (c_{s1} + c_m)(P_{b_{e1r}} + \mathrm{j} P_{b_{e1j}}) + \mathrm{j} i\omega_e c_m (P_{b_{e2r}} + \mathrm{j} P_{b_{e2j}}) \\ &+ (k_{s1} + k_m)(P_{b_{e1r}} + \mathrm{j} P_{b_{e1j}}) - k_m (P_{b_{e2r}} + \mathrm{j} P_{b_{e2j}}) = (S_{b_{e1r}} + \mathrm{j} S_{b_{e1j}}) \end{aligned} \tag{A-100}$$

$$\begin{aligned} &-m_1 i^2 \omega_p^2 (P_{b_{p1r}} + \mathrm{j} P_{b_{p1j}}) - \mathrm{j} i\omega_p (c_{s1} + c_m)(P_{b_{p1r}} + \mathrm{j} P_{b_{p1j}}) + \mathrm{j} i\omega_p c_m (P_{b_{p2r}} + \mathrm{j} P_{b_{p2j}}) \\ &+ (k_{s1} + k_m)(P_{b_{p1r}} + \mathrm{j} P_{b_{p1j}}) - k_m (P_{b_{p2r}} + \mathrm{j} P_{b_{p2j}}) = (R_{b_p 1r} + \mathrm{j} R_{b_{p1j}}) \end{aligned} \tag{A-101}$$

$$-m_1 i^2 \omega_g^2 (P_{b_{g1r}} + \mathrm{j}P_{b_{p1j}}) - \mathrm{j}i\omega_p (c_{s1} + c_m)(P_{b_{p1r}} + \mathrm{j}P_{b_{g1j}}) + \mathrm{j}i\omega_g c_m (P_{b_{g2r}} + \mathrm{j}P_{b_{g2j}}) + (k_{s1} + k_m)(P_{b_{g1r}} + \mathrm{j}P_{b_{g1j}}) - k_m (P_{b_{g2r}} + \mathrm{j}P_{b_{g2j}}) = (R_{b_{g1r}} + \mathrm{j}R_{b_{g1j}}) \tag{A-102}$$

$$-m_2 i^2 \omega_e^2 (P_{b_{e2r}} + \mathrm{j}P_{b_{e2j}}) - \mathrm{j}i\omega_e (c_{s2} + c_m)(P_{b_{e2r}} + \mathrm{j}P_{b_{e2j}}) + \mathrm{j}i\omega_e c_m (P_{b_{e1r}} + \mathrm{j}P_{b_{e1j}}) + (k_{s2} + k_m)(P_{b_{e2r}} + \mathrm{j}P_{b_{e2j}}) - k_m (P_{b_{e1r}} + \mathrm{j}P_{b_{e1j}}) = (S_{b_{e2r}} + \mathrm{j}S_{b_{e2j}}) \tag{A-103}$$

$$-m_2 i^2 \omega_p^2 (P_{b_{p2r}} + \mathrm{j}P_{b_{p2j}}) - \mathrm{j}i\omega_p (c_{s2} + c_m)(P_{b_{p2r}} + \mathrm{j}P_{b_{p2j}}) + \mathrm{j}i\omega_p c_m (P_{b_{p1r}} + \mathrm{j}P_{b_{p1j}}) + (k_{s2} + k_m)(P_{b_{p2r}} + \mathrm{j}P_{b_{p2j}}) - k_m (P_{b_{p1r}} + \mathrm{j}P_{b_{p1j}}) = (R_{b_{p2r}} + \mathrm{j}R_{b_{p2j}}) \tag{A-104}$$

$$-m_2 i^2 \omega_g^2 (P_{b_{g2r}} + \mathrm{j}P_{b_{g2j}}) - \mathrm{j}i\omega_g (c_{s2} + c_m)(P_{b_{g2r}} + \mathrm{j}P_{b_{g2j}}) + \mathrm{j}i\omega_g c_m (P_{b_{g1r}} + \mathrm{j}P_{b_{g1j}}) + (k_{s2} + k_m)(P_{b_{g2r}} + \mathrm{j}P_{b_{g2j}}) - k_m (P_{b_{g1r}} + \mathrm{j}P_{b_{g1j}}) = (R_{b_{g2r}} + \mathrm{j}R_{b_{g2j}}) \tag{A-105}$$

The real and imaginary components are separated on both sides of Eqns. (A-100) through (A-105), to get:
The real component of the backward whirl

$$-m_1 i^2 \omega_e^2 P_{b_{e1r}} + i\omega_e (c_{s1} + c_m) P_{b_{e1j}} - i\omega_e c_m P_{b_{e2j}} + (k_{s1} + k_m) P_{b_{e1r}} - k_m P_{b_{e2r}} = S_{b_{e1r}} \tag{A-106}$$

$$-m_1 i^2 \omega_p^2 P_{b_{p1r}} + i\omega_p (c_{s1} + c_m) P_{b_{p1j}} - i\omega_p c_m P_{b_{p2j}} + (k_{s1} + k_m) P_{b_{p1r}} - k_m P_{b_{p2r}} = R_{b_{p1r}} \tag{A-107}$$

$$-m_1 i^2 \omega_g^2 P_{b_{g1r}} + i\omega_g (c_{s1} + c_m) P_{b_{g1j}} - i\omega_g c_m P_{b_{g2j}} + (k_{s1} + k_m) P_{b_{g1r}} - k_m P_{b_{g2r}} = R_{b_{g1r}} \tag{A-108}$$

$$-m_2 i^2 \omega_e^2 P_{b_{e2r}} + i\omega_e (c_{s2} + c_m) P_{b_{e2j}} - i\omega_e c_m P_{b_{e1j}} + (k_{s2} + k_m) P_{b_{e2r}} - k_m P_{b_{e1r}} = S_{b_{e2r}} \tag{A-109}$$

$$-m_2 i^2 \omega_p^2 P_{b_{p2r}} + i\omega_p (c_{s2} + c_m) P_{b_{p2j}} - i\omega_p c_m P_{b_{p1j}} + (k_{s2} + k_m) P_{b_{p2r}} - k_m P_{b_{p1r}} = R_{b_{p2r}} \tag{A-110}$$

$$-m_2 i^2 \omega_g^2 P_{b_{g2r}} + i\omega_g (c_{s2} + c_m) P_{b_{g2j}} - i\omega_g c_m P_{b_{g1j}} + (k_{s2} + k_m) P_{b_{g2r}} - k_m P_{b_{g1r}} = R_{b_{g2r}} \tag{A-111}$$

The imaginary component of the backward whirl

$$-m_1 i^2 \omega_e^2 P_{b_{e1j}} - i\omega_e (c_{s1} + c_m) P_{b_{e1r}} + i\omega_e c_m P_{b_{e2r}} + (k_{s1} + k_m) P_{b_{e1j}} - k_m P_{b_{e2j}} = S_{b_{e1j}} \tag{A-112}$$

$$-m_1 i^2 \omega_p^2 P_{b_{p1j}} - i\omega_p (c_{s1} + c_m) P_{b_{p1r}} + i\omega_p c_m P_{b_{p2r}} + (k_{s1} + k_m) P_{b_{p1j}} - k_m P_{b_{p2j}} = R_{b_{p1j}} \tag{A-113}$$

$$-m_1 i^2 \omega_g^2 P_{b_{g1j}} - i\omega_g (c_{s1} + c_m) P_{b_{g1r}} + i\omega_g c_m P_{b_{g2r}} + (k_{s1} + k_m) P_{b_{g1j}} - k_m P_{b_{g2j}} = R_{b_{g1j}} \tag{A-114}$$

$$-m_2 i^2 \omega_e^2 P_{b_{e2j}} - i\omega_e (c_{s2} + c_m) P_{b_{e2r}} + i\omega_e c_m P_{b_{e1r}} + (k_{s2} + k_m) P_{b_{e2j}} - k_m P_{b_{e1j}} = S_{b_{e2j}} \tag{A-115}$$

$$-m_2 i^2 \omega_p^2 P_{b_{p2j}} - i\omega_p (c_{s2} + c_m) P_{b_{p2r}} + i\omega_p c_m P_{b_{p1r}} + (k_{s2} + k_m) P_{b_{p2j}} - k_m P_{b_{p1j}} = R_{b_{p2j}} \tag{A-116}$$

$$-m_2 i^2 \omega_g^2 P_{b_{g2j}} - i\omega_g (c_{s2} + c_m) P_{b_{g2r}} + i\omega_g c_m P_{b_{g1r}} + (k_{s2} + k_m) P_{b_{g2j}} - k_m P_{b_{g1j}} = R_{b_{g2j}} \tag{A-117}$$

On combining Eqns. (A-106) through (A-117), we get

$$\mathbf{A}_{bi} \mathbf{p}_{bi} = \mathbf{s}_{bi} \tag{A-118}$$

with

$$\mathbf{A}_{bi} = \begin{bmatrix} \mathbf{A}_{b_{ei}} & 0 & 0 \\ 0 & \mathbf{A}_{b_{pi}} & 0 \\ 0 & 0 & \mathbf{A}_{b_{gi}} \end{bmatrix} \tag{A-119}$$

$$\mathbf{A}_{b_e i} = \begin{bmatrix} -m_1 i^2 \omega_e^2 + (k_{s1} + k_m) & i\omega_e (c_{s1} + c_m) & -k_m & -i\omega_e c_m \\ -i\omega_e (c_{s1} + c_m) & -m_1 i^2 \omega_e^2 + (k_{s1} + k_m) & i\omega_e c_m & -k_m \\ -k_m & -i\omega_e c_m & -m_2 i^2 \omega_e^2 + (k_{s2} + k_m) & i\omega_e (c_{s2} + c_m) \\ i\omega_e c_m & -k_m & -i\omega_e (c_{s2} + c_m) & -m_2 i^2 \omega_e^2 + (k_{s2} + k_m) \end{bmatrix} \tag{A-120}$$

$$\mathbf{A}_{b_p i} = \begin{bmatrix} -m_1 i^2 \omega_p^2 + (k_{s1} + k_m) & i\omega_p (c_{s1} + c_m) & -k_m & -i\omega_p c_m \\ -i\omega_p (c_{s1} + c_m) & -m_1 i^2 \omega_p^2 + (k_{s1} + k_m) & i\omega_p c_m & -k_m \\ -k_m & -i\omega_p c_m & -m_2 i^2 \omega_p^2 + (k_{s2} + k_m) & i\omega_p (c_{s2} + c_m) \\ i\omega_p c_m & -k_m & -i\omega_p (c_{s2} + c_m) & -m_2 i^2 \omega_p^2 + (k_{s2} + k_m) \end{bmatrix} \tag{A-121}$$

$$\mathbf{A}_{b_g i} = \begin{bmatrix} -m_1 i^2 \omega_g^2 + (k_{s1} + k_m) & i\omega_g (c_{s1} + c_m) & -k_m & -i\omega_g c_m \\ -i\omega_g (c_{s1} + c_m) & -m_1 i^2 \omega_g^2 + (k_{s1} + k_m) & i\omega_g c_m & -k_m \\ -k_m & -i\omega_g c_m & -m_2 i^2 \omega_g^2 + (k_{s2} + k_m) & i\omega_g (c_{s2} + c_m) \\ i\omega_g c_m & -k_m & -i\omega_g (c_{s2} + c_m) & -m_2 i^2 \omega_g^2 + (k_{s2} + k_m) \end{bmatrix} \tag{A-122}$$

The displacement and force vectors are given in the matrix form as,

$$\mathbf{p}_{fi} = \begin{Bmatrix} P_{f_{e1ri}} \\ P_{f_{e1ji}} \\ P_{f_{e2ri}} \\ P_{f_{e2ji}} \\ P_{f_{p1ri}} \\ P_{f_{p1ji}} \\ P_{f_{p2ri}} \\ P_{f_{p2ji}} \\ P_{f_{g1ri}} \\ P_{f_{g1ji}} \\ P_{f_{g2ri}} \\ P_{f_{g2ji}} \end{Bmatrix}; \quad \mathbf{s}_{fi} = \begin{Bmatrix} S_{f_{e1ri}} \\ S_{f_{e1ji}} \\ S_{f_{e2ri}} \\ S_{f_{e2ji}} \\ R_{f_{p1ri}} \\ R_{f_{p1ji}} \\ R_{f_{p2ri}} \\ R_{f_{p2ji}} \\ R_{f_{g1ri}} \\ R_{f_{g1ji}} \\ R_{f_{g2ri}} \\ R_{f_{g2ji}} \end{Bmatrix}; \quad \mathbf{p}_{bi} = \begin{Bmatrix} P_{b_{e1ri}} \\ P_{b_{e1ji}} \\ P_{b_{e2ri}} \\ P_{b_{e2ji}} \\ P_{b_{p1ri}} \\ P_{b_{p1ji}} \\ P_{b_{p2ri}} \\ P_{b_{p2ji}} \\ P_{b_{g1ri}} \\ P_{b_{g1ji}} \\ P_{b_{g2ri}} \\ P_{b_{g2ji}} \end{Bmatrix}; \quad \mathbf{s}_{bi} = \begin{Bmatrix} S_{b_{e1ri}} \\ S_{b_{e1ji}} \\ S_{b_{e2ri}} \\ S_{b_{e2ji}} \\ R_{b_{p1ri}} \\ R_{b_{p1ji}} \\ R_{b_{p2ri}} \\ R_{b_{p2ji}} \\ R_{b_{g1ri}} \\ R_{b_{g1ji}} \\ R_{b_{g2ri}} \\ R_{b_{g2ji}} \end{Bmatrix} \tag{A-123}$$